BI-METALLIC PROMOTED VANADYL PYROPHOSPHATE CATALYST FOR PARTIAL OXIDATION OF LIGHT PARAFFIN TO MALEIC ANHYDRIDE

WONG CHUNG SHUNG

MASTER OF SCIENCE

DEPARTMENT OF CHEMICAL ENGINEERING
LEE KONG CHIAN FACULTY OF ENGINEERING AND SCIENCE
UNIVERSITI TUNKU ABDUL RAHMAN
MAY 2017

BI-METALLIC PROMOTED VANADYL PYROPHOSPHATE CATALYST FOR PARTIAL OXIDATION OF LIGHT PARAFFIN TO MALEIC ANHYDRIDE

By

WONG CHUNG SHUNG

A dissertation submitted to the Department of Chemical Engineering,

Lee Kong Chian Faculty of Engineering and Science,

Universiti Tunku Abdul Rahman,

in partial fulfilment of the requirements of the degree of Master of Science

May 2017

ABSTRACT

BI-METALLIC PROMOTED VANADYL PYROPHOSPHATE CATALYST FOR PARTIAL OXIDATION OF LIGHT PARAFFIN TO MALEIC ANHYDRIDE

The vanadyl pyrophosphate (VPO) catalysts prepared via sesquihydrate route were doped with Gadolinium, Lanthanum and Cerium. For the first series, 1.0 mol% of gadolinium and, 1.0 mol%, 3.0 mol% and 5.0 mol% of cerium were added as dopants. For the second series, 1.0 mol% of lanthanum and, 1.0 mol%, 3.0 mol% and 5.0 mol% of cerium were added as dopants. The bi-metallic doped VPO catalysts were produced through calcination in a reaction flow of a mixture of 0.75% *n*-butane in air at 733 K for 24 hours. The catalysts produced in the first series, were denoted as Gd1Ce1, Gd1Ce3 and Gd1Ce5, and for the second series, were La1Ce1, La1Ce3 and La1Ce5. Synthesised catalysts were characterised using XRD, BET, SEM-EDX, ICP-OES, redox titration, TPR in H_2 and catalytic performance tests. XRD diffractogram of Gd-Ce and La-Ce doped catalysts showed similar patterns with major peaks at $2\theta = 22.8^0$, 28.4^0 and 29.8^0, signified the existence of V^{4+} $(VO)_2P_2O_7$ phase at (0 2 0), (2 0 4) and (2 2 1) planes respectively. Gd-Ce doped catalysts were also found to contain $VOPO_4$ phases at $2\theta = 24.9^0$ and 29.2^0, which signified formation of V^{5+} phases. BET analyses result revealed gradual increase in specific surface area from 13.9 m^2g^{-1} to 18.3 m^2g^{-1} with the

addition of higher percentage of Gd-Ce and La-Ce dopants. SEM micrographs showed that addition of increasing percentage of La-Ce dopant resulted in thinner and smaller rosette crystals, and led to higher surface area for catalytic activity. P/V atomic ratio for all the catalysts from ICP-OES and EDX results (P/V=1.17-1.39) were within the optimum range for formation of crystalline $(VO)_2P_2O_7$. Amount of oxygen atoms removed increased with higher concentration of Ce in both Gd-Ce and La-Ce bimetallic doped VPO catalyst due to better synergistic effect between La and Ce dopants towards oxygen reducibility from VPO catalyst. La-Ce doped catalysts exhibited higher catalytic activity towards conversion of *n*-butane to maleic anhydride, with La1Ce5 being the most active catalyst with 41% conversion.

ACKNOWLEDGEMENTS

I would like take this opportunity to express my gratitude to the people who had helped me in my research.

First and foremost, I would like to extend my deepest appreciation to my research supervisors, Dr. Leong and Dr. Sumathi for their unwavering support and continuous dedication in guiding me throughout the research.

Also, I would like to thank the laboratory assistants from UTAR and Mr. Harry Hau from CNG Instruments for their assistance with the laboratory instruments.

I would like to convey my gratitude to UTAR for providing financial support, in the form of UTAR Research Fund, and facilities that are needed to carry out this research.

Last but not least, I would like to thank my family and friends for all of their love and support throughout the duration of the study.

APPROVAL SHEET

This dissertation entitled "**BI-METALLIC PROMOTED VANADYL PYROPHOSPHATE CATALYST FOR PARTIAL OXIDATION OF LIGHT PARAFFIN TO MALEIC ANHYDRIDE**" was prepared by WONG CHUNG SHUNG and submitted as partial fulfillment of the requirements for the degree of Master of Science at Universiti Tunku Abdul Rahman.

Approved by:

_____

(Assc. Prof. Dr. Leong Loong Kong) Date:……

Supervisor

Department of Chemical Engineering

Lee Kong Chian Faculty of Engineering and Science

Universiti Tunku Abdul Rahman

_____

(Assc. Prof. Dr. Sumathi a/p Sethupathi) Date:……

Co-supervisor

Department of Environmental Engineering

Faculty of Engineering and Green Technology

Universiti Tunku Abdul Rahman

FACULTY OF ENGINEERING AND SCIENCE

UNIVERSITI TUNKU ABDUL RAHMAN

Date: _____

SUBMISSION OF DISSERTATION

It is hereby certified that WONG CHUNG SHUNG (ID No: 11UEM04239) has completed this dissertation entitled "**BI-METALLIC PROMOTED VANADYL PYROPHOSPHATE CATALYST FOR PARTIAL OXIDATION OF LIGHT PARAFFIN TO MALEIC ANHYDRIDE**" under the supervision of Assc. Prof. Dr. Leong Loong Kong from the Department of Chemical Engineering, Faculty of Engineering and Science, and Assc. Prof. Dr. Sumathi a/p Sethupathi from the Department of Environmental Engineering, Faculty of Engineering and Green Technology.

I understand that the University will upload softcopy of my dissertation in pdf format into UTAR Institutional Repository, which may be made accessible to UTAR community and public.

Yours truly,

_____

(Wong Chung Shung)

DECLARATION

I hereby declare that the dissertation is based on my original work except for quotations and citations which have been duly acknowledged. I also declare that it has not been previously or concurrently submitted for any other degree at UTAR or other institutions.

_____

(WONG CHUNG SHUNG)

Date _____

TABLE OF CONTENTS

LIST OF TABLES

LIST OF FIGURES

LIST OF ABBREVIATIONS

ºC	Degree Celcius
K	Absolute temperature in Kelvin
Ea	Activation energy
t	Crystallite size for (h k l) phase
λ	X-ray wavelength of radiation for Cu Kα
β_{hkl}	Full-width at half maximum (FWHM) at (h k l) phase
θ_{hkl}	Diffraction angle for (h k l) phase
A_r	Pre-exponential factor
ΔH_1	Heat of adsorption of the first layer
ΔH_2	Heat of liquefaction
ppm	Part-per-million
α_I-, α_{II}-, β-, γ-$VOPO_4$,	Vanadyl phosphate in α_I (alpha I), α_{II} (alpha II), β (beta), and γ (gamma) phases
β-, γ- $(VO)_2P_2O_7$	Vanadyl pyrophosphate in α (alpha), β (beta), and γ (gamma) phases
o-H_3PO_4	*ortho*-Phosphoric acid
α	alpha
β	beta
δ	delta
o	ortho
θ	theta

Å	Angstrom
Al_2O_3	Aluminum oxide
ALMA	Alusuisse Italia-Lummus Crest process
Ar	Argon
Ba	Barium
Be	Beryllium
Bi	Bismuth
BET	Brunauer-Emmett-Teller
C_4	Hydrocarbon
$CH_3(CH_2)_3OH$	1-Butanol
C_4H_{10}	*n*-butane
$C_4H_2O_3$	Furan-2,5-dione
Ca	Calcium
Ce	Cerium
$Ce(NO_3)_3$	Cerium (III) nitrate hexahydrate
Co	Cobalt
CO	Carbon monoxide
CO_2	Carbon dioxide
Cs	Cesium
Cu	Copper
Cu Kα	Copper in K (alpha)
EDX	Energy-dispersive X-ray spectroscopy
EDAX	Energy-dispersive X-ray spectroscopy analysis

ESR	Electron spin resonance spectroscopy
EXAFS	Extended X-ray absorption fine structure
Fe	Ferum
FID	Flame ionisation detector
FWHM	Full-width at half maximum
GC	Gas chromatography
Gd	Gadolinium
GdCe	VPOs catalysts doped with gadolinium and cerium
$Gd(NO_3)_3$	Gadolinium (III) nitrate hexahydrate
GHSV	Gas hourly space velocity
H_2O	Water
H_2SO_4	Sulphuric acid
H_3PO_4	Phosphoric acid
He	Helium
HNO_3	Nitric acid
I_{020}/I_{204}	Intensity ratios of (020) and (204) reflection planes
ICP-OES	Inductively Coupled Plasma-Optical Emission Spectrometry
K	Potassium
$KMnO_4$	Potassium permanganate
La	Lanthanum
LaCe	VPOs catalysts doped with lanthanum and cerium
$La(NO_3)_3$	Lanthanum (III) nitrate hexahydrate

Li	Lithium
MA	Maleic anhydride
Mg	Magnesium
Mo	Molybdenum
MoO_3	Molybdenum oxide
N_2	Nitrogen
Na	Sodium
N_2H_4	Hydrazine
Nb	Niobium
NbPO	Niobium phosphate
$NH_4H_2PO_4$	Ammonium dihydrogen phosphate
$NH_2OH{\cdot}HCl$	Hydroxylammonium chloride
$(NH_4)_2Fe(SO_4)_2{\cdot}6H_2O$	Ammonium iron (II) sulphate
NH_4VO_3	Ammonium (V) metavanadate
O_2	Oxygen
P	Phosphorus
$(PH)_2NH$	Diphenylamine
PO_4	Phosphate
P/V	Phosphorus/vanadium
RSR	Recirculating solid reactor
SEM	Scanning electron microscopy
SiO_2	Silicon oxide

STP	Standard temperature and pressure
T_{max}	Temperature at peak maximum
TCD	Thermal Conductivity Detector
TiO_2	Titanium oxide
TON	Turnover number
TOF	Turnover frequency
TPR	Temperature Programmed Reduction
TPDRO	Temperature Programmed Desorption, Reduction and Oxidation
V	Vanadium
VO_6	Vanadate ion
V_2O_5	Vanadium (V) pentoxide
$VOHPO_4 \cdot 0.5H_2O$	Vanadyl (IV) hydrogen phosphate hemihydrate
$VOHPO_4 \cdot 1.5H_2O$	Vanadyl (IV) hydrogen phosphate sesquihydrate
$VO(H_2PO_4)_2$	*oxo*-Vanadium (IV) dihydrogen phosphate
$(VO)_2P_2O_7$	Vanadyl pyrophosphate
$VO(PO_3)_2$	Vanadium (IV) bis-metaphosphate
$VOPO_4 \cdot 2H_2O$	Vanadyl phosphate dehydrate
VPD	Vanadium phosphorus oxide prepared via dihydrate route
VPO	Vanadium phosphorus oxide
VPOs	Vanadyl pyrophosphate sesquihydrate
XANES	X-ray absorption near edge structure
XRD	X-ray Diffraction

Zn	Zinc
Zr	Zirconium

CHAPTER 1

INTRODUCTION

1.1 Catalyst and Catalysis

Catalyst is an active chemical spectator that participates in chemical reaction but is not consumed. The catalyst produces its effect by lowering the height of the activation barriers by accelerating a reaction without altering the properties of the equilibrated state. Besides that, catalysts can be designed not only to speed up reactions but also to selectively perform its task (Kolasinski, 2008).

Fadoni and Lucarelli (1998) stated that activity of a catalyst is defined as the rate at which a chemical reaction reaches equilibrium. From the standpoint of industry, activity can also defined as the amount of reactant converted into product per unit of time and unit of reactor volume. Selectivity of catalyst is described as the rate of reactant conversion of substrate into desired product. Selectivity usually depends on reaction parameters such as temperature, pressure, reactants composition and also on the catalyst nature.

According to Hartley (1985), the catalysts should have long life span, which means that it can be recycled and used for a longer period. The performance of a catalyst can be measured by the number of moles of product formed per mol in terms of turnover number (TON) and per unit time, giving the turnover frequency (TOF). The TON of catalyst is depending on the activity and stability of the catalyst. By identifying the decomposition path, the lifetime and TON of catalyst can be increased. Similarly, by pinpointing the turnover-limiting step of the catalytic process and enhancing the rate of this specific elementary step, the TOF of a catalyst can be increased (Kurosawa and Yamamoto, 2003).

Catalysis is a cyclical process whereby bonds are formed between catalyst and reacting molecules to generate the product, which will be detached from the catalyst and leaving it unaltered for the next reaction (Chorkendoff and Niemantsverdriet, 2003). As an example, substrates A and B undergo catalytic reaction to generate product P as depicted in Fig. 1.1. Catalysis begins with the bonding of A and B to the catalyst, with both substrate reacting within the complex to form product, P. At the end of the process, P is desorbed from the catalyst without changing the catalyst. The catalyst would then still be in original condition for subsequent reaction.

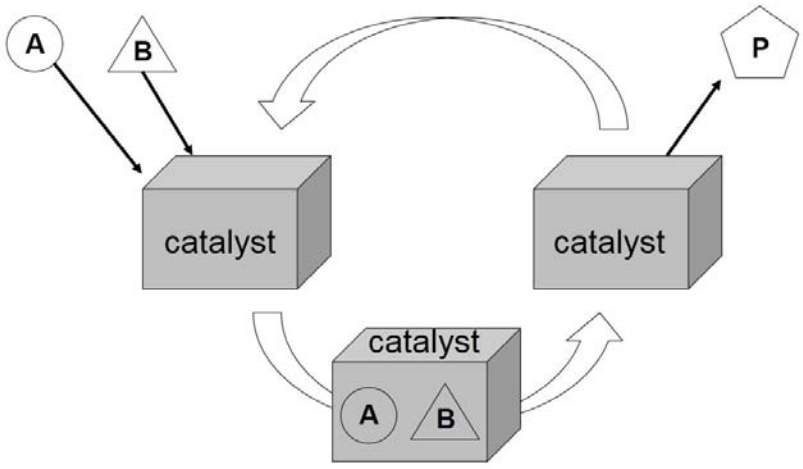

Figure 1.1: Cyclical Process of Catalytic Reaction

As seen from the potential energy diagram in Fig. 1.2, the non-catalysed reaction involves the collision between reactants A and B to produce the product P when sufficient energy is applied to overcome the activation barrier. For the catalysed reaction, spontaneous formation of complex between A and B with the catalyst is exothermic and free energy is lowered. Due to the existence of catalyst in the reaction, the activation energy barrier is lowered and thus, allows the reaction to be more favourable and occur faster at higher rate compared to the non-catalysed reaction. The overall change in free energy for catalysed reaction is equal to the non-catalysed one. Therefore, the catalyst does not affect the equilibrium constant of the overall reaction of $A + B \rightarrow P$.

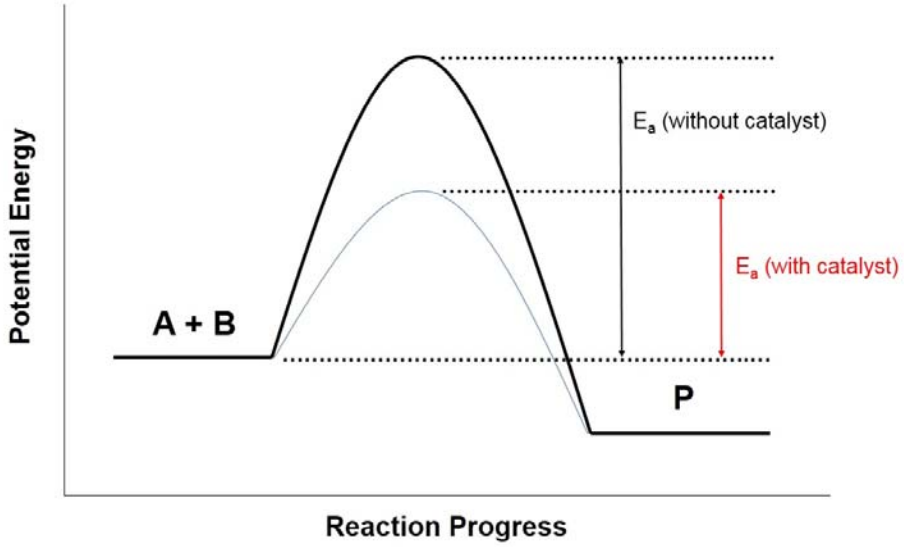

Figure 1.2: Potential Energy Diagram of Catalysed and Non-catalysed Reaction

1.2 Types of Catalyst

Catalyst is generally divided into two types, which are homogeneous and heterogeneous. In a homogeneous reaction, the catalyst is in the same phase as the reactant but for a heterogeneous reaction, the catalyst is in a different phase as the reactant. Biocatalysts such as enzymes are considered as intermediate between both homogeneous and heterogeneous.

1.2.1 Homogeneous Catalyst

Homogeneous catalysis is a term, which describes catalysis where the catalyst is in the same phase as the reactants. The reaction can occur in either gas or liquid phase. Homogeneous catalyst readily mixes into reactant mixture due to the high degree of interaction with reactant, resulting in greater activity and selectivity compared to heterogeneous catalysts. However, it is difficult and costly to recover the catalyst after the reaction due to the catalyst being dispersed in the same phase as reactant, product and solvent. Most homogeneous catalysts are also thermally sensitive and decomposed at temperature below 150 ºC. Several examples of homogeneous catalysis include hydroformylation of olefins, Ziegler-Natta polymerization and C-H activation (Elschenbroich and Salzer, 1992).

1.2.2 Heterogeneous Catalyst

Heterogeneous catalysis describes the catalytic process where the catalyst is in a different phase to the reactants. Heterogeneous catalysts provide a surface for the chemical reaction to take place on. In order for the reaction to occur, one or more of the reactants must diffuse to the catalyst surface and adsorb onto it. After reaction, the products must desorb from the surface and diffuse away from the solid surface. Langmuir-Hinshelwood and Eley-Rideal mechanisms are used to describe at how adsorption takes place at the surface of the catalyst in gas/solid

heterogeneous catalysis. Heterogeneous catalyst has a significant advantage over homogeneous ones due to the ease of separation of catalyst from products and reusability (Chen, 2014). Examples of heterogeneous catalysis are Haber-Bosch ammonia synthesis catalysed by iron, Fischer-Tropsch synthesis with the usage of cobalt/ferum to convert coal to syngas, CO reaction with platinum, palladium and rhodium in catalytic converters in automobiles.

1.3 Sustainable Chemistry

For the past century, the chemical industry has brought much development to modern society. Lives of many people have been greatly improved by increasing the supply of food, medicine, materials and energy, which is made possible by the advancement in chemistry. However, this rapid progression has come with major drawbacks such as environmental and health hazards. Chemical accident such as the Exxon Valdez oil spill in Bligh Reef, Alaska in 1989 has caused immense destruction of the ecosystem in the affected area to date (Maki, 1991). Bhopal disaster in India in 1984, due to leaking of poisonous methyl isocyanate, has resulted in deaths of about 3000 people and more than 40000 injured (de Souza Porto, 1996).

Other than the hazards, chemical industry is also impeded by shortage of resources due to ever-increasing demand. Spiraling production cost and mineral

resource depletion have forced a rethink in resource management. Anastas and Warner (1998) published a set of principles on green chemistry as a guide to address environmental hazard, health impact and, research and development of sustainable chemistry technology.

Major chemical companies are claiming to emphasise more in green and sustainable processes but these sentiments have to be supported by actual results in reaction efficiency, such as reactant conversion, product selectivity and yield over time. Thus, there is a great need for more efficient catalysts, especially in the industry of selective oxidation of hydrocarbons, which will be the main topic of interest in this research.

1.4 Selective Oxidation of Hydrocarbons and Limitations

Valuable chemical products such as acetic acid, acetaldehyde and maleic anhydride have been successfully produced by hydrogenation, dehydrogenation, selective oxidation or total oxidation of hydrocarbons. These transformations are only made possible with the incorporation of catalyst in the reaction. Examples of hydrocarbon reactant, product and the catalyst used in reaction in industry are classified in Table 1.1.

Table 1.1: Examples of Reactant, Product and Catalyst Used in Industry

Reactant	Product	Catalyst	Reference
Methanol	Acetic acid	Lithium and rhodium iodide	Qian et al. (2016)
Propane	Acrolein	Mixed molybdenum, vanadium, tellurium, niobium oxide	Heine et al. (2015)
Isobutene	Methyl methacryalate	Molybdenum and bismuth oxide	Wang et al. (2016)
Benzene	Maleic anhydride	Vanadium pentoxide	Dmuchovsky (1965)

Large petrochemical industries and research bodies have devoted much interest in the studies of catalytic transformation of light alkanes due to the high value of products. One major interest is the selective oxidation of light paraffin to maleic anhydride (MA) over vanadium phosphorus oxide catalysts. The first commercial production of MA was started by National Aniline and Chemical Company and the Weiss and Downs process was employed with benzene as feedstock. However, the usage of benzene has become a major concern to environment, due to the carcinogenic nature of the reactant (Tsai, 2016). Implementation of legislation has resulted in strict control of benzene emissions from MA-producing plants. Benzene is also inherently an inefficient reactant as only four out of six carbon atoms are recovered in the product. With the

advancement of petrochemical industry, C_4 hydrocarbons such as butadiene, *n*-butene and *n*-butane were made available to replace benzene as potential feedstock (Trivedi and Culbertson, 1982).

Bergmann and Frisch (1966) were the first to report that vanadium phosphorus oxide (VPO) was a viable catalyst in transformation of *n*-butane to MA. Despite considerable research effort has been poured in catalysed reaction of C_4 hydrocarbons, the yield was still lower and more expensive than the well-established benzene route. The best performance reported for fixed-bed reactor did not exceed 65% per-pass yield and with a lower conversion rate in fluidised-bed. Ballarini et al. (2006) suggested that one of the factors that could lead to maximisation of MA yield was by modifying the active phase of the catalyst with addition of specific dopants.

1.5 Problem Statement

In recent years, increase in unsaturated polyester resins (UPR) production is observed due to high demand from developing countries. Raw material for UPR production, maleic anhydride is synthesised from *n*-butane using vanadium phosphorus oxide (VPO) catalyst, resulting in greater need for highly active and selective catalyst to alleviate the industry.

Due to the highly selective 14-electron conversion of alkane feedstock to maleic anhydride, most researches were hampered by the low conversion rate and high percentage of by-product. Despite the long history of researches on modification of VPO catalysts and its related fields, the search for the highly active and selective of catalysts is still ongoing.

Previous publications on doped-VPO complexes showed increase in surface density of V=O species, which are considered to be the active sites of partial oxidation of *n*-butane, better control of the oxidation state of vanadium and formation of lattice defects to produce specific surface area for catalytic activity. However, rare earth metals are still relatively untested due to lack of fundamental understanding of their promotion properties on performance of VPO catalysts. As most of the elements from the main groups have been tried as dopant by researchers, rare earth-VPO complex represents a new frontier in VPO research.

1.6 Objectives

This research aims to synthesise a highly active and selective VPO catalysts for partial oxidation of the more environmental-friendly reactant, *n*-butane to produce maleic anhydride. In order to achieve this, the objectives for the research have been set as follows:

i. To synthesise bi-metallic GdCe and LaCe doped VPO catalysts using environmental-friendly reducing agent prepared via sesquihydrate ($VOHPO_4 \cdot 1.5H_2O$) route.

ii. To study the effect of mole percentages of bi-metallic GdCe and LaCe dopants towards the physical, chemical and reactivity of the synthesised catalysts.

iii. To evaluate the catalytic performances of bi-metallic GdCe and LaCe doped catalysts on *n*-butane oxidation to MA.

CHAPTER 2

LITERATURE REVIEW

2.1 Maleic Anhydride and Its Uses

Maleic anhydride (MA) is chemically named as furan-2,5-dione, or cis-butene-dioic anhydride with the formula $C_4H_2O_3$. It has a cyclic structure with carboxylic acid groups next to each other in *cis* form as shown in Figure 2.1. This organic compound is also known by other common names such as toxilic anhydride, maleic acid anhydride or malic acid anhydride. It is a white hygroscopic solid in the form of orthorhombic crystalline needles with a pungent odour.

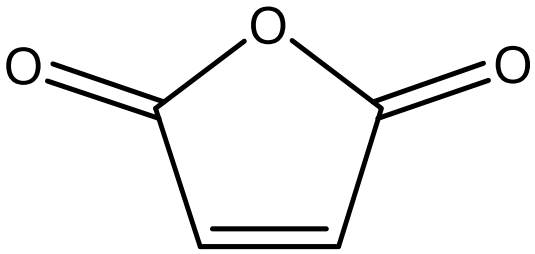

Figure 2.1: Structure of Maleic Anhydride

Maleic anhydride is one of the most important commercial chemical products today. Large percentage of MA produced is used for manufacturing of unsaturated polyester resins in the industry. These resins display properties such as favourable service temperatures, low manufacturing cost and weight, which leads to ease in utilisation in reinforced plastic applications such as automobile, marine craft, building panel, furniture parts, synthetic marble, lightweight pipe and bath tub. High-purity fumaric acid for food applications is also made from refined MA. Fumaric acid is used in paper sizing resins as flavouring agent and food acidulant. It has been also used as nutritional additive and in some indirect applications such as food packaging. In the agriculture sector, MA is used to prepare herbicides, pesticides and plant growth regulators (Lohbeck et al., 2012).

2.2 Market Outlook of Maleic Anhydride

Nearly 70% of the MA is produced by oxidation of *n*-butane, with the remaining percentage is still via benzene route. According to the report in Chemical Week (2003), the annual world consumption of MA in the industry exceeded 1.3 megatonne. Fuelled by the increase of infrastructural development and automobile sales, especially in Asia Pacific region, the global MA market volume swelled to 2.1 megatonne in 2013 (Grand View Research, 2014). Breakdown of global maleic anhydride market share by region is shown in Figure 2.2.

The revenue generated for MA sale that year was 4.3 billion US dollars. 30% of the market share of MA is held by major producers such as Huntsman Corporation, Sasol-Huntsman, Polynt S.p.A, Lanxess Corporation, Nippon Shokubai Co. Ltd., Flint Hills Resources LP, Marathon Petroleum Co. LLC and Mitsui Chemicals, Inc. Market volume of MA is projected to hit 2.8 megatonne by 2018.

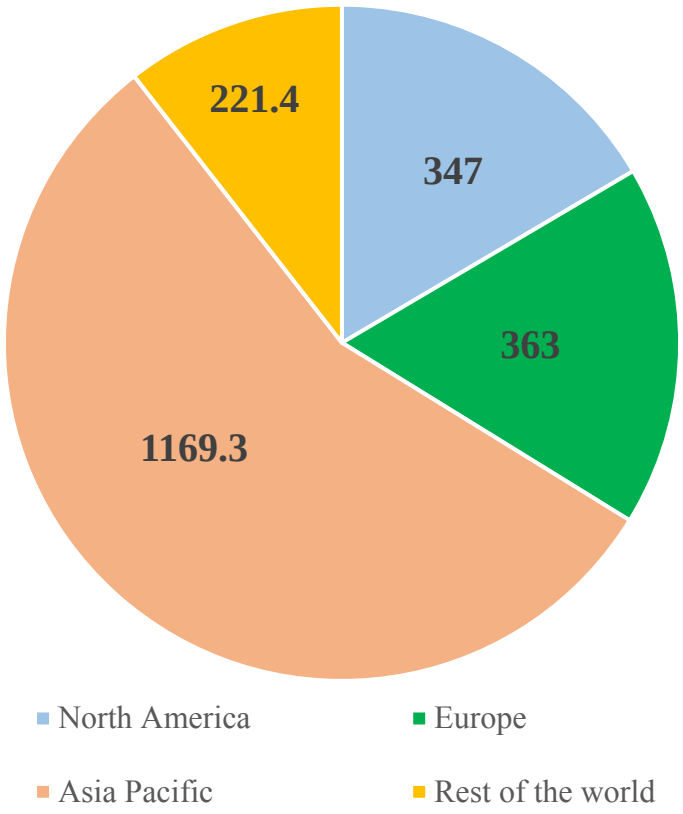

Figure 2.2: Global Maleic Anhydride Market Volume in Tonne by Region in 2013

2.3 Formation of Maleic Anhydride

In the early 1930s, MA is synthesised by selective vapour phase oxidation of benzene reactant over vanadium pentoxide and molybdenum trioxide catalysts as illustrated in Figure 2.3.

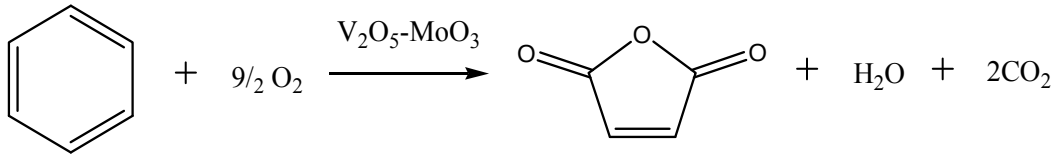

Figure 2.3: Oxidation of Benzene to Maleic Anhydride

The benzene route has been slowly replaced with the cleaner and efficient C_4 hydrocarbons such as *n*-butane. MA is produced from a 14-electron selective oxidation of *n*-butane over vanadium phosphorus oxide (VPO) catalysts. Felthouse (2001) described that selective oxidation of *n*-butane involves the abstraction of 8 hydrogen atoms, insertion of 3 oxygen atoms and formation of a 5-membered ring on the surface of VPO catalyst. The simplified overall reaction is shown below as Equation 2.1:

$$C_4H_{10} + \frac{7}{2}O_2\ (\text{air}) \longrightarrow C_4H_2O_3 + 4H_2O \quad (2.1)$$

In reality, the *n*-butane oxidation mechanism comprises of much more complex multiple steps and produces less observed intermediates. Cavani and Trifiro (1994) reported that, firstly, butanes, butadiene and furan were detected in the oxidation of *n*-butane with vanadium phosphorus oxide catalysts under selected conditions such as deficiency of oxygen at very high *n*-butane concentration, and secondly, the oxidation of butanes, butadiene, and furan was under the same conditions as for *n*-butane oxidation, maleic anhydride and all the intermediates of with the exceptions of 2,5-dihydrofuran and lactone. The step by step conversion and reaction type proposed by Cavani and Trifiro is tabulated in Table 2.1 and illustrated in Figure 2.4.

Table 2.1: Proposed Steps of the Mechanism of Selective Oxidation of *n*-Butane to Maleic Anhydride

Conversion reaction	Type of reaction
n-butane to *n*-butenes	Oxidative dehydrogenation
n-butenes to butadiene	Allylic oxidation
Butadiene to 2,5-dihydrofuran	1,4-oxygen insertion
2,5-dihydrofuran to furan	Allylic oxidation
Furan to lactone	Electrophilic oxygen insertion
Lactone to Maleic Anhydride	Electrophilic oxygen insertion

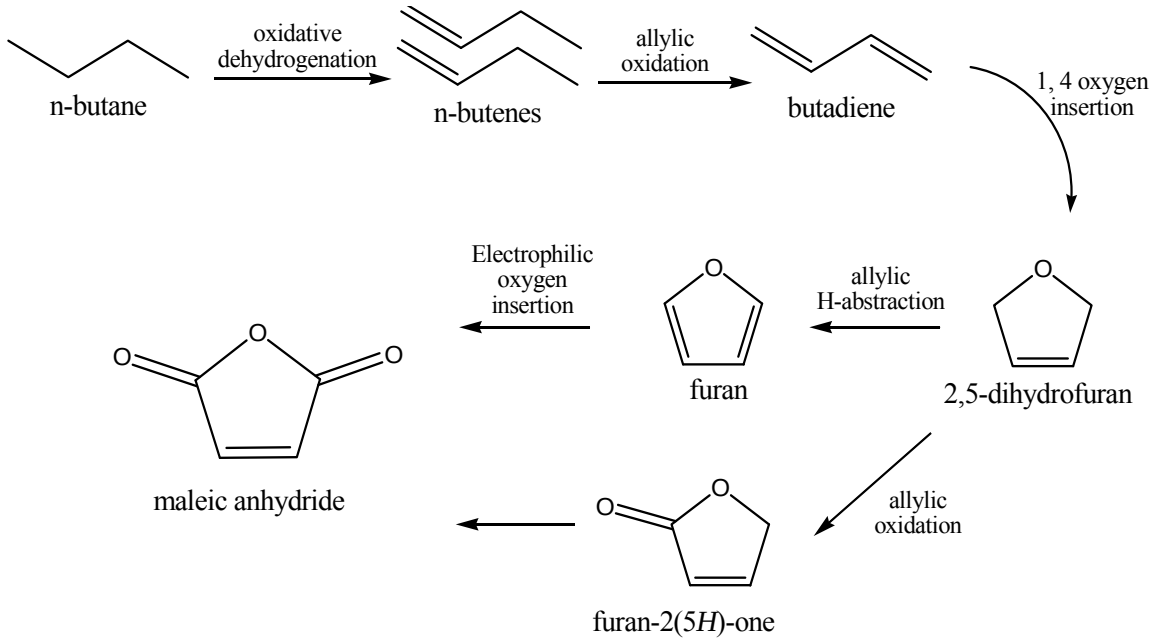

Figure 2.4: Schematic Diagram of the Mechanism of Selective Oxidation of *n*-Butane to Maleic Anhydride

2.4 Reactor Technology for Maleic Anhydride Production

Generally, there are three different types of processes employed in the commercial production of MA; fixed-bed processes, fluidised-bed processes and recirculating-solids process. Some of the MA industry's processes and the type of reactor employed with the recovery method are summarised in Table 2.2.

Table 2.2: Examples of Industrial Processes for MA Production

Process	Type of reactor	Recovery method	Reference
ALMA	Fluidised-bed	Anhydrous	Romano et al. (2016)
Sohio-UCB	Fluidised-bed	Aqueous	Trifiro and Grasselli (2014)
Mitsubishi	Fluidised-bed	Aqueous	Yates and Lettieri (2016)
Monsanto	Fixed-bed	Anhydrous	Trifiro and Grasselli (2014)
Denka-Scientific	Fixed-bed	Aqueous	Homma and Kitaoka (2014)
DuPont	Transported bed	Aqueous	Romano et al. (2016)

Recirculating solid reactor (RSR) was developed by Monsanto and DuPont using the transported bed technology. RSR operated at lower conversion of reactant to maleic anhydride but higher selectivity compared to fixed-bed and fluidised-bed processes (Bither, 1984). The DuPont process is divided into two parts: in the first part, *n*-butane is fed and oxidised by the catalyst in a riser. The outlet stream will contain the mixture of *n*-butane, CO_X, MA and the reduced catalyst. In the second part, the reduced catalyst will be recovered by cyclone and transported to the regenerator reactor for re-oxidation of catalyst for subsequent reactions. MA is then recovered using water. One advantage of this technology is the absence of oxygen in the feed, which prevent the formation of flammable mixture and permits the process to work with high concentration of *n*-butane. The oxygen needed for the oxidation of *n*-butane is extracted from the VPO catalyst instead (Contractor, 1991).

Fluidised-bed reactor technology also generated high productivity of MA due to possibility of operating at high inlet concentration of *n*-butane feed. This process allows reaction temperature to be controlled uniformly by passing the reactant through the catalyst in fluid with high velocity. One of the most advanced fluidised-bed technology employed in the industry is the Alusuisse Italia-Lummus Crest (ALMA) process. In the recovery section of this reactor, organic solvent is used to extract MA from the reaction effluent gas. Conversely, there are several disadvantages such as *n*-butane back-mixing, which reduces the selectivity of MA, and high mechanical stress on the catalyst (Centi, 2001).

Structurally, the fixed-bed reactor consist of multiple tubes that are packed with coarse catalysts. A certain volume of pressure of 1-2 bar is applied at the inlet to maintain the flow rate across the reactor. Due to the exothermic nature of the *n*-butane oxidation reaction, cooling sections are setup in the determined hotspots of the reactor in order to prevent overheating of the catalyst and reactor tubes. Schematic diagram of the Huntsman fixed-bed reactor is shown in Figure 2.5. To date, this reactor technology is the best among the three other fixed-bed processes. Denka-Scientific Design fixed-bed process reported 83% conversion of *n*-butane and 54% selectivity to MA. In this process, 1.7% of *n*-butane in air is fed to the fixed-bed reactor under the temperature of 673 K. Crude MA is recovered using adsorption in water to form maleic acid, which is then distilled in *ortho*-xylene to obtain pure MA.

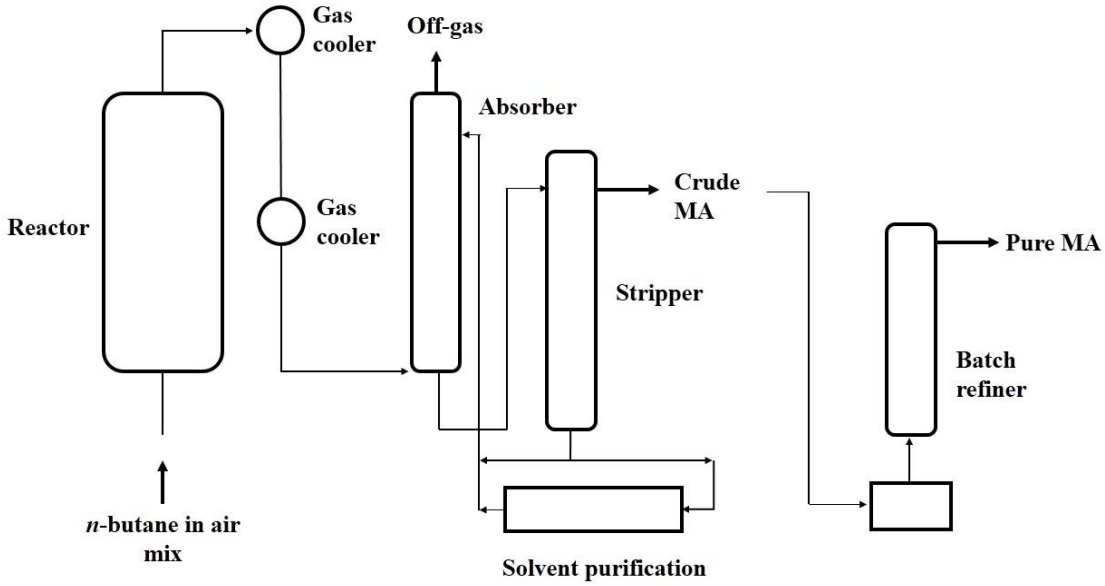

Figure 2.5: Schematic Diagram of Huntsman Fixed-bed Process (Kwon and Stanecki, 1994)

2.5 Vanadium Phosphorus Oxide (VPO) Catalyst

Vanadium phosphorus oxide (VPO) is a unique and complex catalytic system. Centi et al. (1988) explained that VPO catalysts were first noted as being effective example of commercial catalyst for selective oxidation of *n*-butane oxidation to maleic anhydride. This is because VPO catalyst contains vanadyl pyrophosphate, $(VO)_2P_2O_7$ active sites that allow the oxidation to occur (Bergmann and Frisch, 1966). An activated VPO catalyst can also consist of other VPO phases such as $VOHPO_4 \cdot 0.5H_2O$, α_I-, α_{II}-, β-, γ-, δ-$VOPO_4$, $VOPO_4 \cdot 2H_2O$, $VO(H_2PO_4)_2$ and $VO(PO_3)_2$ of +5, +4 and +3 oxidation states (Bordes, 1987; Centi, 1993).

Hutchings (1991) explained that ideal molecular structure of $(VO)_2P_2O_7$ phase contained sheets of elementary units of single PO_4 tetrahedra and a pair of VO_6 octahedra that are connected with each another at the edges on the (0 2 0) plane. Misono (2002) deduced further that the (0 2 0) basal plane, where the V-O-V pair sites located, was responsible for the selective oxidation of *n*-butane to maleic anhydride. The crystal faces of the selective and non-selective oxidation sites were displayed in Figure 2.6.

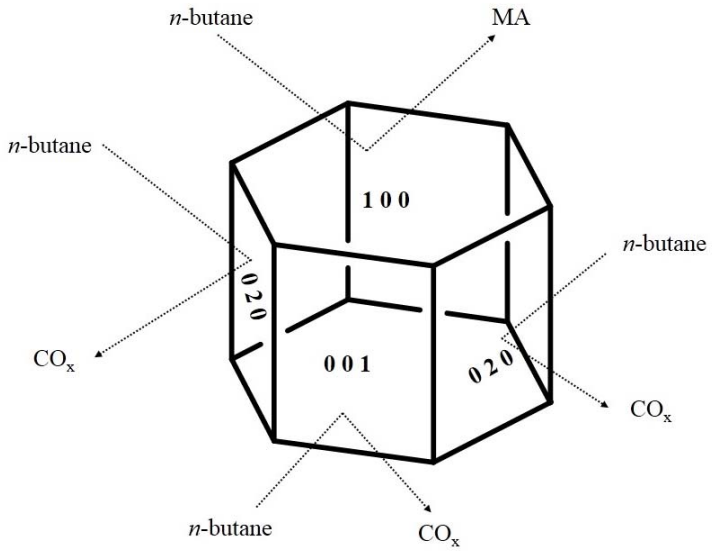

Figure 2.6: Crystal Faces of $(VO)_2P_2O_7$ for Oxidation of *n*-Butane

Witko et al. (2001) conducted a comprehensive study on the electronic structure of the $(VO)_2P_2O_7$ phase and created a realistic model of the phase on the (1 0 0) surface as illustrated in Figure 2.7. Their study has presented that the strong nucleophilicity of surface oxygen studies correspond to interaction of adsorbate with $(VO)_2P_2O_7$ phase on (1 0 0) plane, thus leading to activation of organic species.

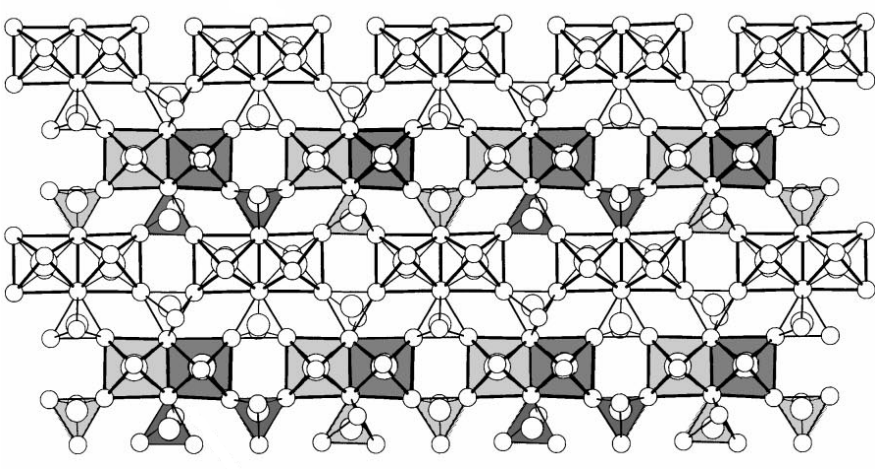

Figure 2.7: Structure of $(VO)_2P_2O_7$ along (1 0 0) Plane

2.6 Parameters that Affect Characteristics of VPO Catalyst

There are many direct and indirect factors influencing the characteristics and the performance of a VPO catalyst. Nevertheless, the review was focused on the parameters that will affect the VPO catalysts listed as below:

i. Type of reducing agent and precursor

ii. Calcination temperature, duration and environment

iii. Comparative relation between phosphorus and vanadium, P/V ratio

iv. Support system

v. Dopant

2.6.1 Type of Reducing Agent and Precursor

Across the years, few notable routes of production of $(VO)_2P_2O_7$ catalyst have been proposed and tested, such as the dihydrate ($VOPO_4 \cdot 2H_2O$), hemihydrate ($VOPO_4 \cdot 0.5H_2O$) and sesquihydrate ($VOPO_4 \cdot 1.5H_2O$) method. VPO catalysts are produced via aqueous method with hydrochloric acid as reducing agent, organic method with benzyl alcohol and isobutanol as reducing agents, dihydrate method with the reaction of $VOPO_4 \cdot 2H_2O$ and isobutanol, and sesquihydrate method with the reaction of $VOPO_4 \cdot 2H_2O$ with 1-butanol.

For aqueous technique, mineral agent such as HCl and N_2H_4, is used as reducing agent and water (H_2O) as medium, with addition of H_3PO_4 in the preparation of catalyst, in meanwhile, for organic technique, different types of alcohols such as methanol and isobutanol is used as reducing agent (Abon and Volta, 1997).

From the experiments conducted by Shima and Hatano (1997), they deduced that catalyst prepared in an organic method was more active than catalyst prepared in aqueous method. This was because, the surface area of a catalyst prepared by non-aqueous medium was in the range of 20-50 m^2g^{-1}, which was much higher compared to the one prepared in aqueous medium. Cavani et al. (1984) also stated that catalyst produced via organic method had lower oxidability in air, thus

making it possible to obtain the selective compound of vanadium (IV) β-phase. The higher the surface area of catalyst also makes it possible to oxidise *n*-butane at a lower temperature. This is consistent with the finding by Bremer and Dria (1983), whereby preparation in organic media is better compared to aqueous media. The research resulted in production of catalysts having higher activity for oxidation of *n*-butane to produce maleic anhydride. The catalysts also exhibit higher intrinsic surface area compared to aqueous-derived catalysts.

According to Hutchings et al. (1997), they found that isobutanol used in the second step to reduce the $VOPO_4 \cdot 2H_2O$ to $VOHPO_4 \cdot 0.5H_2O$, which is also called as the VPD route, could synthesise good catalyst precursors with better morphology and texture. The VPD method can produce the $(VO)_2P_2O_7$ phase with the highest surface platelet morphology exposing preferentially the active plane (1 0 0) for maleic anhydride formation. It was also reported that using $VOPO_4 \cdot 2H_2O$ as starting point, the form of $VOHPO_4 \cdot 0.5H_2O$ that can be topotactically transformed to a high surface area final catalyst comprising mainly of $(VO)_2P_2O_7$, can be produced. Besides that, this method also provides a new route to the synthesis of $VO(H_2PO_4)_2$ which provide ultra-selective catalysts for maleic anhydride production.

Typically, most of the conventional and industrial vanadyl pyrophosphate catalysts are produced via hemihydrate route, $VOHPO_4 \cdot 0.5H_2O$. It is a good

precursor because of the ease of synthesis of hemihydrate with a high growth of (0 0 1) plane which produces (1 0 0) plane in $(VO)_2P_2O_7$. The plane is active for selective oxidation of *n*-butane to maleic anhydride. Quoting from various sources, Mizuno and co-workers had also reported that there were four general methods of preparation of $VOHPO_4 \cdot 0.5H_2O$ precursor; first, reduction of V_2O_5 with various alcohols, followed by reaction with H_3PO_4. Second method was reaction of mixture of V_2O_5 and H_3PO_4 with $NH_2OH \cdot HCl$ or oxalic acid and followed by heat treatment at 403 K (Mizuno et al., 1997). Third method was the VPD route conducted by Hutchings et al. (1997), and fourth method was hydrothermal synthesis with V_2O_4 and H_3PO_4 at 773 K. In all, first, second and third methods consist of two steps while fourth method requires high temperature of 773 K.

Another method of preparation of $VOHPO_4 \cdot 0.5H_2O$ precursor using a simple one-step solvothermal process was devised by Rownaghi and Taufiq-Yap (2010). V_2O_5 and H_3PO_4 were reacted with an aliphatic alcohol (1-propanol or 1-butanol) at high temperatures (373-423 K) in a high pressure autoclave, and the precursor will be synthesised directly. This method can reduce preparation time and lowers the production temperature by 50%. In the same journal, Taufiq-Yap and Rownaghi too reported that when the catalysts were prepared using this novel method, the yield of maleic anhydride increased to 38% compared to conventional prepared catalyst with 21%.

Another novel method of preparation is via the sesquihydrate route and this method is considerably new in the field of VPO catalyst research. A new phase, $VOHPO{\cdot}1.5H_2O$ can be produced by reduction of $VOPO_4{\cdot}2H_2O$ with 1-butanol (Matsuura et al., 1995). Taufiq-Yap et al. (2004) employed the procedure of reducing $VOPO_4{\cdot}2H_2O$ with 1-butanol and activated the reaction at 753 K over 10 hours on-stream to produce the sesquihydrate precursor with high specific activity in gas-phase oxidation of *n*-butane.

2.6.2 Calcination Temperature, Duration and Environment

According to Cheng and Wang (1996), calcination atmospheres will affect the catalyst morphology and vanadium valence. Therefore, the type of calcination environment needs to be chosen in accordance with the oxidability of VPO catalyst precursors to achieve the optimised performance. It is further indicated that the unpromoted catalyst needs to be calcined in a more oxidizing atmosphere compared to a promoted one, in order to achieve optimum yield.

Calcination at certain temperature is necessary to produce an amorphous state with both V^{5+} and V^{4+} phases in catalysts. The amorphous state can then be dehydrated and transformed to other oxidised phases after the introduction of reactant mixture (Cavani and Trifiro, 1994b). Hodnett and colleagues (1983) also reported that, by increasing the calcination temperature, P/V ratio, at which a

mixture of phases observed, can be shifted to higher values. Higher calcination temperatures also found to be favouring the formation of β-$VOPO_4$ and resulted in lower surface area. Waugh and Taufiq-Yap (2003) too had mentioned that catalysts calcined for a longer period of time had clearer and more prominent rosette-shape agglomerates compared to less calcined catalysts. However, calcination temperature and duration should not be too high. Cavani and Trifiro (1994b) also added that care must be taken to avoid excess oxidation of amorphous phase to V^{5+} phase and to prevent sintering in the catalyst.

Mallada et al. (2000) discovered that reacting catalysts with *n*-butane at different reactor positions will result in differing yield. The catalysts were progressively reduced along the bed, and even surface V^{3+} phases were observed in catalyst situated at furthermost reactor positions. The reduced catalysts became highly unselective as available oxygen was used mainly to burn the maleic anhydride formed near the reactor.

2.6.3 P/V Ratio

One of the most influential parameter of the VPO catalyst synthesis is comparative relation between phosphorus and vanadium, P/V ratio. An optimal catalyst composition will present a slight excess of phosphorus with respect to stoichiometric value of the precursor (Horowitz et al., 1988).

By employing a standard method of preparation but with variable P/V ratios, Hodnett et al. (1983) have concluded that, low P/V ratios will favour the formation of β-$VOPO_4$ with average oxidation state of vanadium (V_{AV}) values close to +5, whereas high P/V ratios will favour the formation of βα with V_{AV} values close to +4. The research by Bergeret et al. (1987) is in agreement with that finding. They also noticed a decrease in crystallinity of the catalyst with the increase of P/V ratio.

With excess of free H_3PO_4 adsorbed on the precipitate to P/V = 1, the decomposition of $(VO)_2P_2O_7$ was delayed and β-phase was completely oxidised to β-$VOPO_4$ (Poli et al., 1981). However, they stressed that calcination temperature and method of preparation, together with the effect of P/V ratio, will produce catalysts of different morphologies.

2.6.4 Support System

Small metal particles are often unstable and prone to sintering, especially in extreme conditions. Therefore, a promoter can provide structural support to catalysts. Some of the more widely applied promoter in industry are silica, alumina and titania. Alumina is very much a preferred support material in the industry as it combines high surface area, favourable pore structure and strong mechanical

stability. Furthermore, alumina is an inexpensive and readily available material (Kolasinski, 2008).

In general, a promoter should have three functions; first, as textural promoters which inhibit the growth of small particles of active phase during use, second, as electronic and structural promoters, which may dissolve in active phase and alter its electronic character and third, as poison-resistant promoters, which can shield the active phase from poisoning by impurities (Bond, 1987).

There has been much evidence to show that promoter affects the performance of VPO catalysts. According to Shyamal and Rao (1992), the promoted catalyst showed better performance compared to unpromoted catalyst at higher reaction temperature, higher contact time and higher inlet *n*-butane concentration. It was shown that a highly dispersed and largely amorphous V-P oxide phase can be stabilised on a low-area pigmentary anatase. Metal oxides promoters like TiO_2, SiO_2 and Al_2O_3 were used as inert material to disperse the active phase to form a support system, while hoping it can increase the surface area of active phase to achieve higher activity (Taufiq et al. 2007).

2.6.5 Dopant

Dopants are materials that can enhance the effect of catalyst. They can be divided into structural dopants and electronic dopants. Extensive studies have been conducted over the years to search for suitable dopants that can increase the activity and selectivity of VPO catalysts.

Sant and Varma (1993) deduced that low levels of zirconium (ratio Zr/V = 0.03) decreased the temperature of maximum yield in comparison to unpromoted sample. The primary role of zirconium could be to increase the surface area of the catalyst or to alter the oxygen mobility by a small measure.

Abdelouahab et al. (1995) found that both Co and Fe dopants strongly improved the selectively to maleic anhydride compared to the undoped catalyst but *n*-butane conversion was decreased for Co and increased for Fe. Doping VPO by Co^{3+} had strongly enhanced the V^{5+}/V^{4+} ratio at the surface due to favourable potential redox value whereas Fe^{3+} decreased this ratio.

It was reported that incorporation of alkali and alkaline earth metal ions such as Li, Na, K, Cs, Be, Mg, Ca and Ba at different concentrations, which easily donate electrons to the framework of vanadium phosphorus structure, leads to an

increase of the effective negative charge on oxygen atom and of the rate of *n*-butane oxidation. This might be due to the presence of dopant that causes an increase of surface P/V ratio and corresponding changes of acidic properties of the catalysts (Zazhigalov et al., 1996).

The addition of NbPO improved the catalytic performance of VPO catalysts for *n*-butane oxidation to maleic anhydride. Addition of Nb to VPO catalysts showed improvement in mechanical strength of VPO pellets. It also influenced the V^{5+}/V^{4+} ratio at both $VOHPO_4 \cdot 0.5H_2O$ precursor and of the $(VO)_2P_2O_7$ catalyst (Oliveira et al., 2000).

Xu et al. (2002) found that VPO system doped by a set of Mo, Zr and Zn elements and synthesised in aqueous medium, was found to be highly selective in *n*-butane oxidation. Combination of three elements might create a synergetic influence on the VPO catalyst that may result in high maleic anhydride selectivity and maintaining activity in fair butane conversion.

Bi-promoted catalysts produced via sesquihydrate route have better catalytic performance in terms of high selectivity. Bi was found to be a good structural promoter as it increased the surface area of the catalyst. Bi-promoted catalysts also showed six to nine times higher amounts of oxygen evolved compared to non-promoted catalyst (Leong et al., 2010).

Molybdenum facilitates easy desorption of products from catalyst surface; it maintains optimal defect concentration and blocks the non-selective sites. The presence of Mo leads to increase exposure of (1 0 0) planes and the defects. Mo also reported to be responsible for decreasing of crystallite size of $VOHPO_4 \cdot 0.5H_2O$, which led to increase in surface area (Narayana et al., 2004). It has long been known that Mo can be added to VPO catalysts for improved performances, as cited by Felthouse et al. (1997). However, preparation of precursor with aqueous media has been outpaced by other newer medias, therefore Mo has been suggested to VPO catalysts in non-aqueous media under optimal Mo/V ratios of about 0.01 to 0.0.5. It was also found that by incorporating trace amount of Mo into VPO precursor, after activated, the catalyst will significantly reduce the acrylic acid content of the reaction product gas exiting a reactor in which maleic anhydride is produced by oxidation of *n*-butane.

Addition of bimetallic dopant, Ce and Bi led to promotion of catalyst performance in terms of activity and selectivity compared to bulk VPO catalyst with the *n*-butane conversion of 78%. This study by Rownaghi et al. (2009) also showed that addition of low percentages of La and Ce resulted in increase of oxidation state of vanadium, which resulted to higher selectivity to MA.

CHAPTER 3

MATERIALS AND METHODOLOGY

3.1 Gases and Materials for Preparation of Catalysts

Gases and materials with the brand and purity used for the preparation of the catalysts in this research are listed in Table 3.1.

Table 3.1: Gases and Materials for Preparation of Catalysts

Gas/Material	Brand	Purity (%)
Vanadium (V) pentoxide, V_2O_5	Merck	99
ortho-Phosphoric acid, *o*-H_3PO_4	Merck	85
1-Butanol, $CH_3(CH_2)_3OH$	Merck	99.5
0.75 % *n*-Butane in air	Malaysia Oxygen Berhad (MOX)	0.75
Gadolinium (III) nitrate hydrate, $Gd(NO_3)_3$	Alfa Aesar	99.9
Cerium (III) nitrate hexahydrate, $Ce(NO_3)_3$	Alfa Aesar	99.5
Lanthanum (III) nitrate hexahydrate, $La(NO_3)_3$	Alfa Aesar	99.9

3.2 Methodology

The catalysts for this research were prepared by the sesquihydrate route. This route was selected to prepare the catalysts as the reducing agent used, 1-butanol is considered as an environmental-friendly route compared to the other routes. Method of preparation of the sesquihydrate precursor, $VOHPO_4 \cdot 1.5H_2O$ is based upon the previous work done by Leong et al. (2012) and Taufiq-Yap et al. (2004). The prepared sesquihydate precursor was divided into two portions and used to prepare modified vanadyl pyrophosphate sesquihydrate (VPOs) catalysts in two different series.

Rare-earth metals, gadolinium (Gd), lanthanum (La) and cerium (Ce) were added as dopant to the sesquihydrate precursor with the expectation to improve the performance of the catalyst in terms of *n*-butane conversion and selectivity to MA. Preparation technique for the doped VPOs catalysts is based on the previous study done by Rownaghi et al. (2009). In the first series of this research, 1.0 mol% of Gd was added with 1.0, 3.0 and 5.0 mol% of Ce as bi-metallic dopants to modify the VPOs catalysts. In the second series, 1.0 mol% of La was added with 1.0, 3.0 and 5.0 mol% of Ce as bi-metallic dopants to modify the VPOs catalysts. Three repetitions of the experimental set of every catalyst sample were prepared to ensure accuracy. The concentration of 1.0, 3.0 and 5.0 mol% were chosen on the basis of initiating the research by employing the lowest significant concentration of 1.0 mol% of dopant before increasing it to 3.0 and 5.0 mol% to conserve resources.

3.2.1 Preparation of GdCe and LaCe Doped VPOs Catalysts

Vanadium pentoxide, V_2O_5 (15.0 g, Merck) was suspended in *ortho*-phosphoric acid, *o*-H_3PO_4 (90.0 ml, 85%, Merck) and deionised water (24.0 ml/g solid). The suspension was refluxed under continuous stirring at 393 K for 24 hours. The resultant yellow solids, vanadyl phosphate dihydrate ($VOPO_4 \cdot 2H_2O$), were centrifuged and oven-dried at 373 K for 48 hours. Then, 10.0 g of $VOPO_4 \cdot 2H_2O$ solids were suspended in 1-butanol (150.0 ml, Merck). For the first series, 1.0 mol% of gadolinium nitrate, $Gd(NO_3)_3$ and 1.0 mol% of $Ce(NO_3)_3$ were added into the suspension using wetness impregnation technique. This process was repeated with 3.0 and 5.0 mol% of $Ce(NO_3)_3$. For the second series, 1.0 mol% of lanthanum nitrate, $La(NO_3)_3$ and 1.0 mol% of $Ce(NO_3)_3$ were added into the suspension using wetness impregnation technique. This process was repeated with 3.0 and 5.0 mol% of $Ce(NO_3)_3$. The mixtures from both series were refluxed under continuous stirring at 393 K for 8 hours. Resultant light blue solid precursors, vanadyl phosphate sesquihydrate ($VOHPO_4 \cdot 1.5H_2O$) were centrifuged and oven-dried at 373 K for 24 hours. The dried precursors were calcined in a reaction flow of 0.75% *n*-butane in air mixture at 733 K for 24 hours to produce the activated GdCe and LaCe doped vanadyl pyrophosphate sesquihydrate, VPOs catalysts. The preparation process is illustrated in Figure 3.1 and the colour changes at different stages of preparation are shown in Figure 3.2.

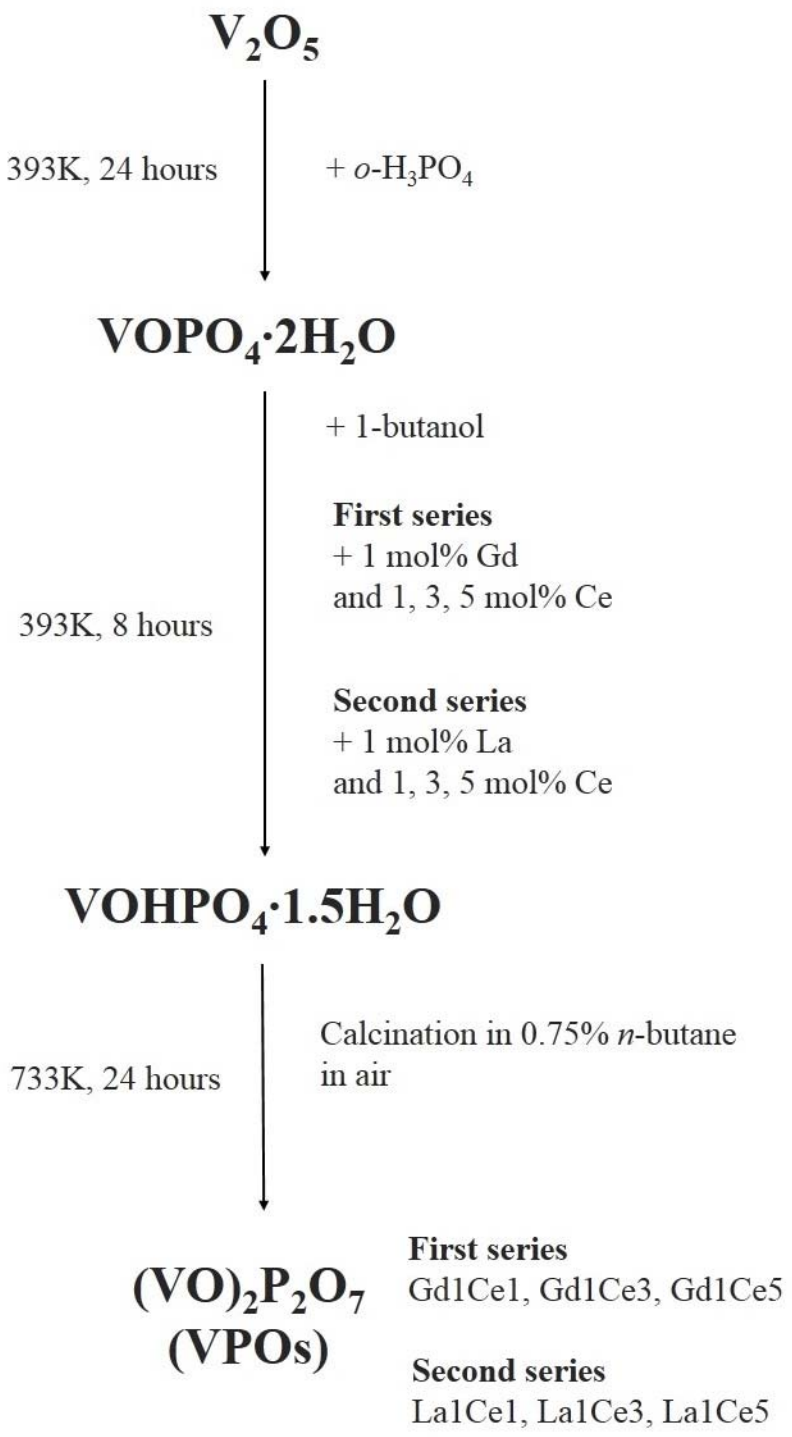

Figure 3.1: Flowchart of Preparation of GdCe and LaCe Doped VPOs Catalysts

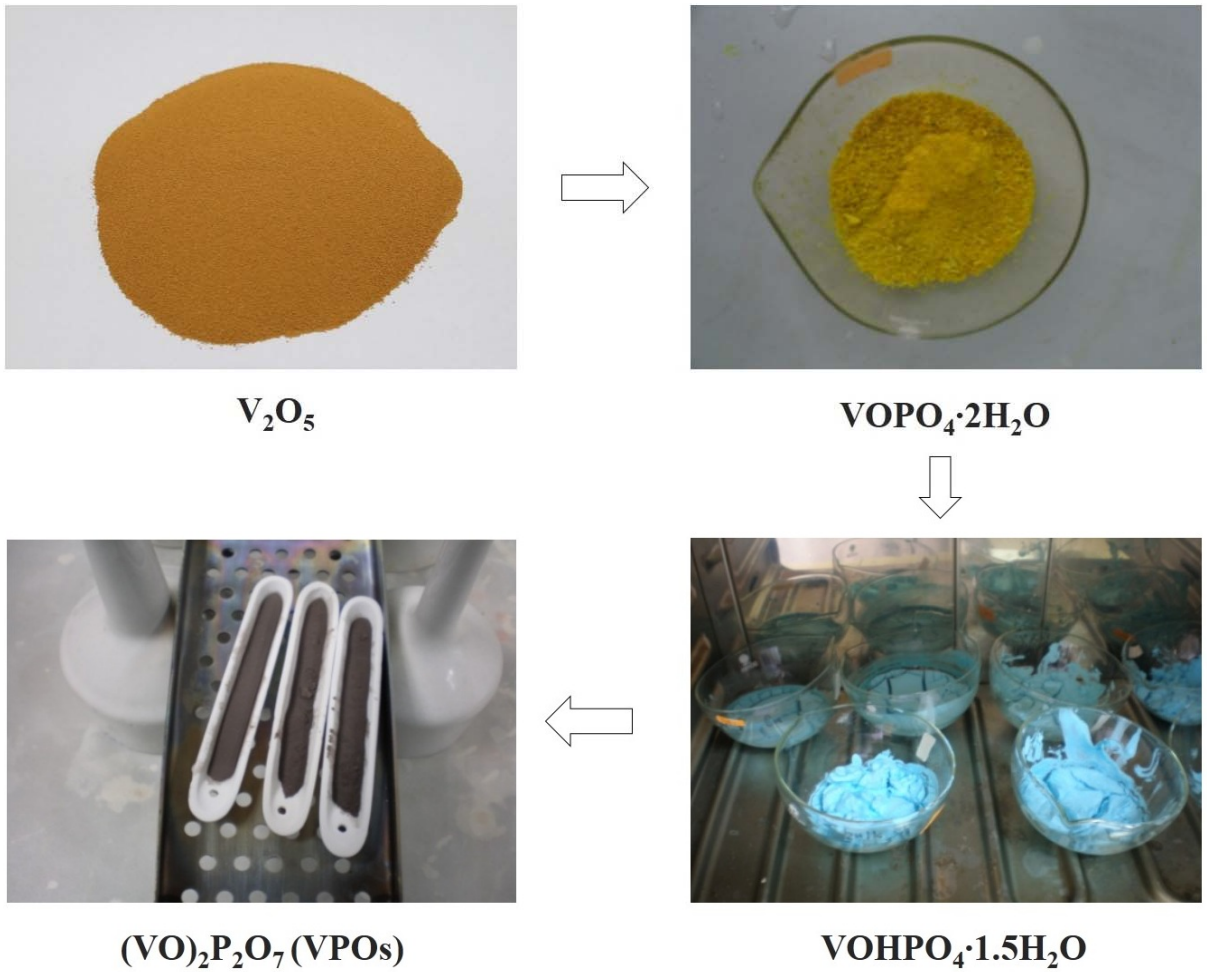

Figure 3.2: Colour Changes at Different Stages during the Preparation of GdCe and LaCe Doped Catalysts

3.3 Chemicals, Gases and Instruments for Characterisation of Catalysts

Chemicals and gases used for the respective characterisation tests of the synthesised vanadyl pyrophosphate catalysts are listed in Table 3.2.

Table 3.2: Chemicals and Gases Used for Characterisation Tests

Characterisation test		Supplier	Purity (%)
BET surface area measurement			
Chemicals	Liquid nitrogen, N_2	Linde	
Gases	Purified nitrogen, N_2	MOX	99.999
	Purified helium, He	MOX	99.999
ICP-OES			
Chemicals	Nitric acid, HNO_3	Merck	70
	Vanadium (V) pentoxide, V_2O_5	Merck	99
	ortho-Phosphoric acid, H_3PO_4	Merck	85
	Ammonium (V) metavanadate, NH_4VO_3	BDH	
	Ammonium dihydrogen phosphate, $NH_4H_2PO_4$	Univar	
Redox titration			
Chemicals	Potassium permanganate, $KMnO_4$	Fisher	
	Sulphuric acid, H_2SO_4	Merck	95-97
	Diphenylamine, $(Ph)_2NH$	Acros	
	Ammonium iron (II) sulphate, $(NH_4)_2Fe(SO_4)_2 \cdot 6H_2O$	Systerm	
Temperature-programmed reduction (TPR) in H_2			
Gases	Hydrogen in argon, H_2/Ar	MOX	5.23
	Purified argon, Ar	MOX	99.999
Catalytic test			
Gases	*n*-Butane in air	MOX	1.0
	Purified helium, He	MOX	99.999
	Purified oxygen, O_2	MOX	99.999
	Purified argon, Ar	MOX	99.999
	Purified nitrogen, N_2	MOX	99.999

The instruments employed to run the respective characterisation tests of the synthesised vanadyl pyrophosphate catalysts are listed in Table 3.3. All of the doped GdCe and LaCe doped VPO catalysts were subjected to three repetition tests for every characterisation test to obtain the average result for better accuracy.

Table 3.3: Characterisation Tests and the Instruments Used

Characterisation test	Specification
Physical characterisation	
X-ray diffractometer	Shimadzu XRD-6000
Scanning electron microscopy (SEM)	Hitachi S-3400N
Brunauer-Emmett-Teller (BET) surface area measurement	Thermo Finnigan Sorptomatic 1990
Chemical characterisation	
Redox titration	Burette and conical flask
Energy dispersive X-ray (EDX)	EDAX software
Inductively coupled plasma-optical emission spectrometry (ICP-OES)	Perkin Elmer Optima 2000 DV Optical Emission Spectrometer
Reactivity study	
Temperature-programmed reduction (TPR)	TPDRO 1100
Catalytic test	Fixed-bed microreactor with on-line Thermo Scientific TRACE-GC Ultra

3.4 Characterisation Techniques

3.4.1 X-ray Diffraction (XRD) Analysis

X-ray diffraction analysis was performed with a Shimadzu model XRD-6000 diffractometer in order to determine the phase compositions of the catalysts under normal atmospheric condition and at ambient temperature. The radiation applied is Cu Kα (λ = 1.54 Å) at 40 kV generated by a copper X-ray tube (Toshiba, A-40-Cu) at normal focus 2.0 kW. Powdered catalysts were placed uniformly on shallow aluminium sample holder and scanned within the range of 2θ = 2.0-60.0º at the rate of 2.0º per minute. The patterns obtained from the diffractogram were matched up with the Joint Committee on Powder Diffraction Standards (JCPDF) database version 2.6 to determine the phases of the catalysts. Full-width at half maximum (FWHM), intensity and unique distance (d-spacing) values were obtained using Basic Process software version 2.6. Crystallite size of the catalysts can be calculated using the Scherrer equation (3.1):

$$t = \frac{0.89\lambda}{\beta_{hkl}\cos\theta_{hkl}} \qquad (3.1)$$

t = crystallite size for (h k l) phase

λ = X-ray wavelength of radiation for Cu Kα

β_{hkl} = FWHM at (h k l) phase

θ_{hkl} = diffraction angle for (h k l) phase

3.4.2 Brunauer-Emmett-Teller (BET) Surface Area Measurement

BET measurement was used to determine the total specific surface area of the catalysts at low temperature of 77 K. Thermo Finnigan Sorptomatic 1990 nitrogen adsorption-desorption analyser was employed to carry out the measurement. About 0.5 g of powder catalyst was placed in a sealed quartz tube and degassed overnight at 423 K to eliminate water and foreign molecules from the surface of the catalyst. After the degassing, the pretreated catalyst sample was maintained at 77 K in liquid nitrogen bath. The sample was then subjected with flow of gaseous nitrogen by the analyser under wide range of pressures. The amount of nitrogen adsorbed was measured and plotted into adsorption/desorption isotherm by the analyser's internal software. The isotherm graphs of all of the catalysts were attached in Appendix I. The specific surface area of the catalyst was calculated using the BET equation (3.2) proposed by Brunauer et al. (1938):

$$\frac{p}{V(p_o - p)} = \frac{1}{V_m C} + \frac{(C-1)p}{CV_m p_o} \qquad (3.2)$$

V = volume at standard temperature and pressure (STP) of gas adsorbed per unit mass of adsorbent at a given pressure, p and constant pressure

p_o = saturation pressure at measurement temperature

V_m = volume of gas required to form a complete monolayer adsorbed layer at STP per unit mass of adsorbent when the surface is covered by a monolayer of adsorbate.

C = free energy of adsorption constant which represented by the equation (3.3) below

$$C = A_r \exp\left(\frac{(\Delta H_1 - \Delta H_2)}{RT}\right) \qquad (3.3)$$

Ar = pre-exponential factor, s^{-1}

ΔH_1 = heat of adsorption of the first layer, $Jmol^{-1}$

ΔH_2 = heat of liquefaction, $Jmol^{-1}$

R = gas constant, 8.314 $JK^{-1}mol^{-1}$

T = absolute temperature in K

3.4.3 Scanning Electron Microscopy (SEM) and Energy Dispersive X-ray (EDX) Spectroscopy

Surface morphology of the catalysts were determined by the micrographs generated using the Hitachi S-3400N scanning electron microscope. Trace amount of catalyst sample was fixed on an aluminium stub of the sample holder using carbon tape. The stub was coated with palladium and gold using a sputter coater to

prevent charging of the catalyst sample with electron beam, thus enhancing the micrograph image quality. The atoms of the surface of catalyst were excited by electrons sent by the analyser and the particles emitted from the surface were collected by the detector. The micrograph of the scanned catalyst will be displayed and, saved for surface morphology deduction and energy dispersive X-ray (EDX) analysis.

EDX analyses were carried out using the EDAX software from the Ametek EDX instrument linked with the SEM. The specific wavelength emissions resulted from the excitation of surface of the catalysts were fed to the EDX instrument to generate the atomic structure data of the phosphorus and vanadium. Thus, the ratio between phosphorus and vanadium, P/V can be calculated as a result.

3.4.4 Redox Titration

Redox titration was performed to determine the average oxidation state of vanadium of the catalyst using the method developed by Niwa and Murakami (1982). About 0.1 g of catalyst was dissolved in 100 ml of concentrated sulphuric acid, H_2SO_4 (2 M) at 353 K and cooled to room temperature for titration. 20.0 ml of the dissolved solution was titrated with potassium permanganate, $KMnO_4$ solution (0.01 N) to oxidise V^{3+} and V^{4+} in the solution to V^{5+}. The end point was reached when the colour of the solution changed from greenish blue to pink. Volume of $KMnO_4$ solution used was recorded as V_1. The pink, oxidised solution

was treated further with a second titration with ammonium iron (II) sulphate, $(NH_4)_2Fe(SO_4)_2{\cdot}6H_2O$ solution (0.01 N) to reduce V^{5+} to V^{4+} in the solution. Diphenylamine was used as an indicator in the second titration. The end point was reached when the colour of the solution changed from purple to colourless. Volume of $(NH_4)_2Fe(SO_4)_2{\cdot}6H_2O$ solution used was recorded as V_2. A fresh 25.0 ml of the original dissolved catalyst solution was subjected to a third titration with $(NH_4)_2Fe(SO_4)_2{\cdot}6H_2O$ solution (0.01 N) to determine the amount of V^{5+} in the original solution. Diphenylamine was also used as an indicator in the third titration. The end point was reached when the colour of the solution changed from purple to greenish blue. Subsequently, the volume of $(NH_4)_2Fe(SO_4)_2{\cdot}6H_2O$ solution used was recorded as V_3. Amount of V^{3+}, V^{4+} and V^{5+} and the average oxidation state of vanadium (V_{AV}) can be then calculated by solving the equations by Niwa and Murakami (1982) (3.4) below:

$$V^{3+} = 20(0.01)V_1 - 20(0.01)V_2 + 20(0.01)V_3$$

$$V^{4+} = 40(0.01)V_2 - 40(0.01)V_3 - 20(0.01)V_1$$

$$V^{5+} = 20(0.01)V_3$$

$$V_{AV} = \frac{5V^{5+} + 4V^{4+} + 3V^{3+}}{\left(V^{5+} + V^{4+} + V^{3+}\right)} \qquad (3.4)$$

3.4.5 Inductively Coupled Plasma-Optical Emission Spectrometry (ICP-OES) Analysis

The Perkin Elmer Optima 2000 DV Optical Emission Spectrometer was employed to conduct quantitative and qualitative analysis on the catalysts to provide insight on chemical composition of the catalysts. The analyte was prepared by dissolving 0.025 g of catalyst in 10.0 mL of 8 M nitric acid, HNO_3 and stirred under low heating. The analyte solution was diluted with deionised water to the concentration of 100 ppm. Phosphorus, P and vanadium, V standard solutions were prepared by water dilution of ammonium dihydrogen phosphate, $NH_4H_2PO_4$ and ammonium metavanadate, NH_4VO_3 respectively, to the concentrations of 10, 20 and 40 ppm. Deionised water was prepared as blank solution that served as control solution. All standard and blank solutions were added with the same concentration of 10.0 mL of 8 M HNO_3 in order to be consistent with the analyte solutions. At the beginning of the analysis, the analyte was pumped into an analytical nebuliser and aspirated directly inside the plasma flame. After losing the electrons, the molecules of the sample were broken into their respective atoms and yielded radiation at certain characteristic wavelengths of P and V elements. Hence, the ratio between phosphorus and vanadium, P/V can be calculated from the concentration units data evolved from the characterisation.

3.4.6 Temperature-Programmed Reduction (TPR) in H_2

Temperature-programmed reduction (TPR) in H_2 was used to determine the amount of reducible oxygen species with different oxidation states and, structural changes of the catalysts upon cyclic reduction and re-oxidation processes. Thermo Electron TPDRO 1100 was utilised to perform the reduction analyses.

To prepare the catalyst for analysis, trace amount of the catalyst was placed in a quartz tube sandwiched between two layers of quartz wool. A thermal conductivity detector, TCD was placed at the exit of the tube. In the first stage, the catalyst was subjected to a pre-treatment process in a flow of purified argon at 1 bar, 20 cm^3 min^{-1} and held for 5 minutes at room temperature. In the second stage, the catalyst was pre-treated further in a flow of purified argon at 1 bar, 20 cm^3 min^{-1} and under incremental heating from room temperature to 473 K for 45 minutes, and cooled to room temperature after that. The two stages of pre-treatment was carried out to remove impurities that might interfere with the results. In the third stage, the pre-treatment process was switched to the analysis one. The catalyst was reduced in a flow of 5.23% hydrogen in argon at 1 bar, 25 cm^3 min^{-1} under incremental heating from room temperature to 1000 K at the rate of 5 K per minute. Hydrogen consumption was monitored and measured by the detector. The consumption data was plotted into TPR in H_2 profile by the TPDRO software.

3.4.7 Catalytic Test

Catalytic performance tests on the catalysts were carried out using a laboratory-scaled fixed-bed microreactor. About 0.25 g of catalyst was inserted into a reactor tube and plugged together with quartz wool. A thermocouple was placed at the center of the catalyst bed with the reaction temperature set to ±1 K. *n*-Butane and compressed air were fed simultaneously into the reactor with the stream concentration fixed to 1 % *n*-butane in air by a calibrated mass flow controller. The oxidation of 1 % *n*-butane in air was carried out at 673 K with GHSV = 2400 h^{-1}. The resultant reactants and products from the oxidation were fed through heated lines to the on-line Thermo Scientific TRACE GC Ultra gas chromatograph for analysis. The GC was equipped with a HayeSep R packed column (1 m, 1/8 inch) and molecular sieve 5A column (3 m, 1/8 inch). In the columns, gaseous molecules such as CO, CO_2, O_2, H_2O and N_2 were separated and detected by a TCD. Maleic anhydride and *n*-butane were separated in a RTX-1701 wide bore capillary column (30 m, 0.53 mm) and detected by a flame ionisation detector (FID). From the gas chromatography data analyses, the percentage of *n*-butane conversion and, product selectivity of maleic anhydride and carbon oxides can be determined.

CHAPTER 4

RESULTS AND DISCUSSION

4.1 Series 1: Effect of Gd and Ce Bi-metallic dopants on the Physico-chemical and Catalytic Properties of Vanadyl Pyrophosphate Catalysts via Sesquihydrate Route

In the first series of this study, vanadyl pyrophosphate (VPOs) catalysts were prepared via the sesquihydrate route with Gd and Ce bi-metallic dopants added in varying mol percentages. Concentration of Gd was fixed to 1.0 mol% and concentration of Ce varied between 1.0, 3.0 and 5.0 mol%. The activated catalysts were denoted as GdXCeY (X = 1, Y = 1, 3, 5 mol%), with Gd1Ce1, Gd1Ce3 and Gd1Ce5 being synthesised. The effect of different combination percentages of Gd and Ce dopants on the physico-chemical, reactivity and catalytic properties of the VPOs catalysts were studied. Bulk VPOs-R8, prepared by Leong et al. (2012), was designated as control sample and its experimental data were used as comparison in all analyses in this series of study.

4.1.1 Series 1: XRD Analyses

From the patterns obtained from the XRD analyses, Figure 4.1 shows the three main reflection peaks appeared at 2θ = 22.8º, 28.4º and 29.0º, which

corresponded to (0 2 0), (2 0 4) and (2 2 1) planes respectively, for all bi-metallic GdCe doped VPOs catalysts (JCPDS File No. 34-1381). These peaks were corresponded to the crystalline $(VO)_2P_2O_7$ phase, V^{4+} and responsible for the oxidation of *n*-butane to MA.

Two other weaker peaks were also detected in the XRD pattern in Figure 4.1 at 2θ = 25.1º and 29.3º for the GdCe doped VPOs catalysts (JCPDS File No. 34-1247), which corresponded to the amorphous α_{II}-$VOPO_4$, V^{5+} phase. XRD study on bi-metallic Ce-Co and Ce-Bi doped VPO catalysts prepared via conventional method by Rownaghi et al. (2009) also found similar $(VO)_2P_2O_7$ and $VOPO_4$ phases. However, the $VOPO_4$ phase found in their study was β-$VOPO_4$ type, which was known to induce deleterious effect and will result to lower catalytic performances. In comparison, the α_{II}-$VOPO_4$ phase found in GdCe doped catalysts in this study were considered to be responsible for good activity and selectivity for oxidation of *n*-butane to MA. Effect of the tetragonal α_{II}-$VOPO_4$ and orthorhombic β-$VOPO_4$ phases on catalytic performances of VPO catalyst have been explained in previous researches by Bordes (1987) and Kiely (1995). This revelation proved that the addition of Gd, together with Ce, could produce a positive synergistic effect and result in formation of good α_{II}-$VOPO_4$ phase.

Crystallite sizes of (0 2 0) and (2 0 4) planes were calculated from its full-width half maximum (FWHM) values. From the XRD data in Table 4.1, it was observed that the crystallite size along the (0 2 0) reflection plane increased

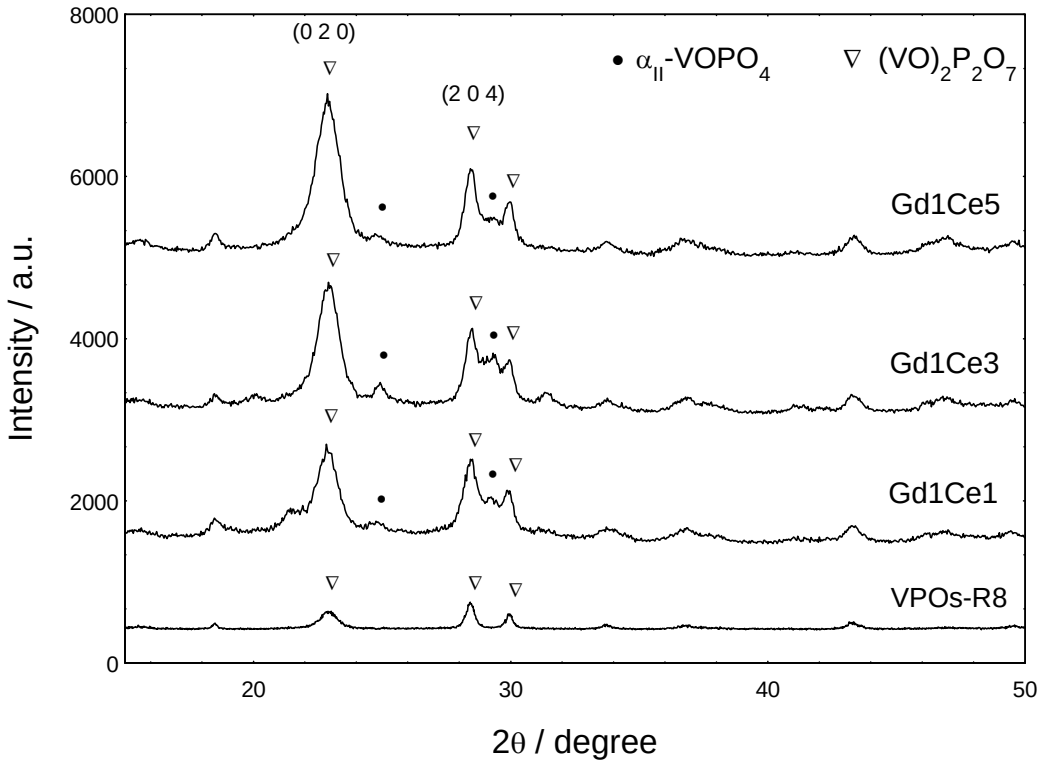

Figure 4.1: XRD Patterns for Bulk and GdCe Doped VPOs Catalysts

Table 4.1: XRD Data of Bulk and GdCe Doped VPOs Catalysts

Catalyst	Line width[a] (°)		Crystallite size[b] (Å)		I_{020}/I_{204}[c]
	(0 2 0)	(2 0 4)	(0 2 0)	(2 0 4)	
VPOs-R8	0.7400	0.3869	108.28	209.37	0.52
Gd1Ce1	1.1191	0.7121	71.59	113.78	0.63
Gd1Ce3	1.0207	0.8554	78.49	94.71	0.82
Gd1Ce5	1.0017	1.3249	80.00	61.19	1.31

[a]FWHM of (0 2 0) and (2 0 4) reflection planes
[b]Crystallite size by means of Scherrer equation
[c]Intensity ratio between (0 2 0) and (2 0 4) reflection planes

gradually from 71.59 to 78.49 Å and 80.00 Å. However, an opposite trend was observed for the crystallite size at (2 0 4) plane, with a decrease from 113.78 Å to 94.71 Å and 61.19 Å for the same series of catalysts. This showed that, as the mol% of Gd dopant in the catalyst was fixed, the increase of mol% of Ce dopant has contributed to the changes to the microsctructure of the VPOs catalysts. By comparison, the crystallite sizes of bulk VPOs catalyst were significantly higher than the doped catalysts at 108.28 Å and 209.37 Å, along the (0 2 0) and (2 0 4) planes, respectively. The same incremental in intensity ratio of (0 2 0) and (2 0 4) planes, I_{020}/I_{204} also indicated the presence of more vanadyl group on the surface of the catalyst due to higher exposure of (0 2 0) plane, which could lead to improvement on catalytic performance as explained by Zazhigalov et al. (1996) and Haber et al. (1997).

4.1.2 Series 1: BET Surface Area and Chemical Analyses

The results from BET surface area measurement, ICP-OES, EDX and redox titration for the GdCe doped VPOs catalysts were discussed in this section. All of the data from chemical analyses are tabulated in Table 4.2.

From the data accumulated from BET measurement, the specific surface area increased from 13.97 m^2g^{-1} to 16.52 m^2g^{-1} and 17.11 m^2g^{-1}. As the mol% of Ce dopant increased, it was observed that the increasing trend in specific surface area is directly related to the reduction of crystallite size along the (2 0 4) plane.

Table 4.2: Specific Surface Area, Chemical Compositions, Average Oxidation Numbers and Percentages of V^{4+} and V^{5+} Oxidation States Present in Bulk and GdCe Doped VPOs Catalysts

Catalyst	Surface area (m^2g^{-1})	P/V ratio (ICP-OES)	P/V ratio (EDX)	Average oxidation number of vanadium		
				V^{4+} (%)	V^{5+} (%)	V_{AV}
VPOs-R8	19.00	1.03	1.12	95.81	4.19	4.0419
Gd1Ce1	13.97	1.17	1.25	92.62	7.38	4.0738
Gd1Ce3	16.52	1.21	1.26	82.73	17.27	4.1727
Gd1Ce5	17.11	1.39	1.42	82.81	17.19	4.1719

This pattern is in accordance to the previous research done by Rownaghi et al. (2010) whereby smaller crystallite size contributed to higher surface area for effective *n*-butane oxidation. From here, it can be deduced that Ce is an effective structural promoter of the (1 0 0) basal face of $(VO)_2P_2O_7$ phase. In contrast, the specific surface areas of the GdCe doped catalysts were lower than the bulk catalyst. This could be attributed to the existence of dopants, which are known to alter the morphology of the VPOs catalyst. Addition of Gd and Ce have induced the formation of bulkier structure, thus resulting to lower surface area. Similar effect of dopants on the surface area of catalyst has also been observed in previous research by Taufiq-Yap (2006).

Chemical analyses using ICP-OES showed that the stoichiometric P/V atomic ratio for Gd1Ce1, Gd1Ce3 and Gd1Ce3 were 1.17, 1.21 and 1.39 respectively. From the EDX analyses, it can be observed that the P/V atomic ratio were ranging from 1.25 to 1.42. The P/V atomic ratio results of the GdCe doped VPOs catalysts were slightly higher than the optimal range (P/V $\geq$ 1.0) for producing of $(VO)_2P_2O_7$ phase (Centi, 1993). It was also noted that the P/V atomic ratios of the GdCe doped VPOs catalysts were higher than the undoped bulk catalyst. This indicated that the increasing mol% of Ce contributed to the excess of phosphorus on the bulk and surface of the catalysts. The excess of phosphorus allowed better stabilisation of $(VO)_2P_2O_7$, V^{4+} phase on the catalysts and would result in higher activity (Centi et al. 1988). This phenomenon was reflected in the higher number oxygen atoms removed in TPR analyses and higher percentage of *n*-butane conversation in catalytic tests for Gd1Ce3 and Gd1Ce5 catalysts.

From the redox titration results, the average oxidation number of vanadium, V_{AV} for Gd1Ce1, Gd1Ce3 and Gd1Ce5 were calculated as 4.0738, 4.1727 and 4.1719, respectively. The increment in V_{AV} of the GdCe doped catalysts was due to the increase in amount of V^{5+} species, which was observed in the XRD patterns. Bulk VPOs-R8 was found to have the lowest V_{AV} of 4.0419, which pointed to lesser amount of V^{5+} phase in the undoped catalyst. The synergistic effect of Gd-Ce assisted in the promotion of amorphous V^{5+} phase, which would lead to a bulkier structure of the VPOs catalyst.

4.1.3 Series 1: SEM Analyses

Surface morphologies of GdCe doped VPOs catalysts were examined by scanning electron microscopy (SEM). Retrieved micrographs are shown in Figure 4.2 (a)-(c). The doped VPOs catalysts displayed similar secondary structure of plate-like crystals in various sizes that were agglomerated into rosette-shaped clusters. These rosette-shaped aggregates consisted of $(VO)_2P_2O_7$ platelets that were exposed preferentially of the (1 0 0) plane as explained by Kiely et al. (1995).

As seen in Figure 4.2 (a), rough and thick plate-like crystals were agglomerated and formed. This phenomenon explained the smaller surface area observed in BET measurement. The bulky nature of the crystals due to the presence of amorphous V^{5+}, α_{II}-$VOPO_4$ phase, was also correctly anticipated by the XRD results and chemical analyses results. As 3.0 and 5.0 mol% of Ce were added, the size of the platelets decreased and agglomerated into smaller rosette clusters with folded edges, which led to higher surface area. Again, this occurrence displayed in Figure 4.2 (b) and 4.2 (c) was consistent with the BET surface area analyses. Identical, but smaller rosette-shaped crystals were detected in the SEM micrograph of undoped bulk VPOs-R8 catalyst. This was due to the absence of significant V^{5+} phase, as compared to the GdCe doped catalysts, and led to less bulky structure for the bulk catalyst. This observation on the morphology explained the higher surface area of the bulk catalyst as opposed to the GdCe catalysts.

(a)

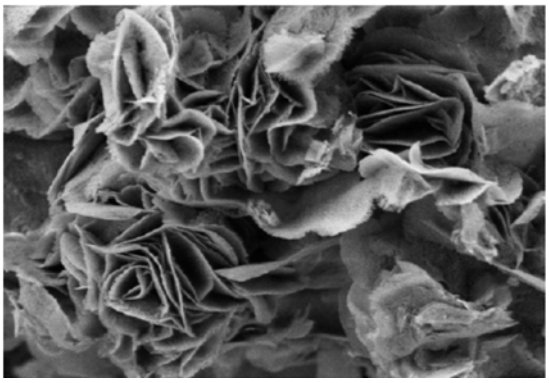

(b)

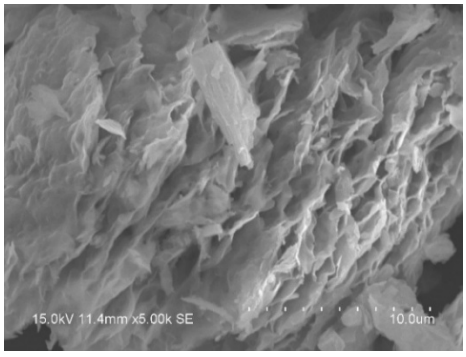

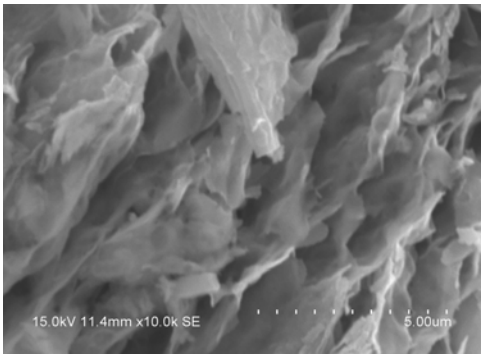

(c)

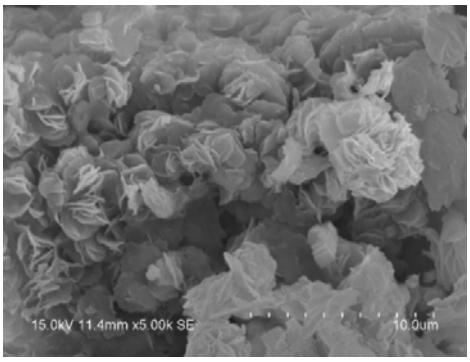

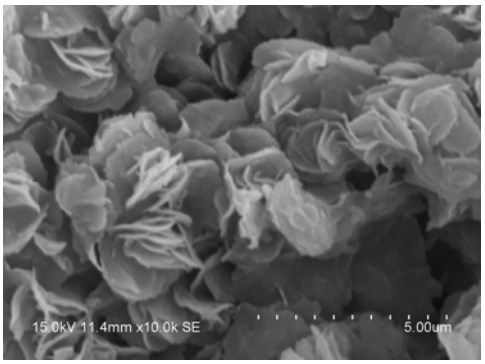

(d)

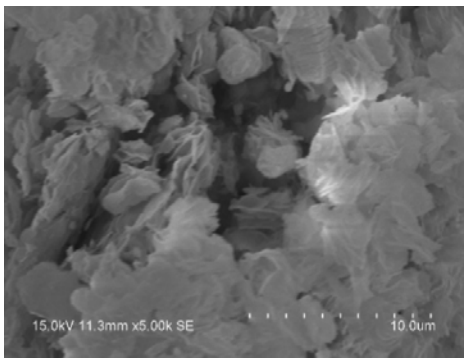

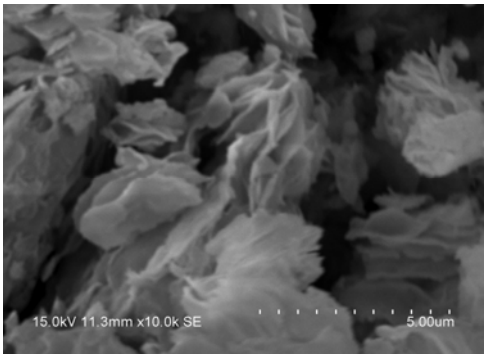

Figure 4.2: SEM Micrographs of (a) VPOs-R8 (b) Gd1Ce1 (c) Gd1Ce3 and (d) Gd1Ce5 Catalysts (Magnification × 5000 and 10000)

4.1.4 Series 1: TPR in H_2 Analyses

Figure 4.3 shows the TPR profiles for GdCe bi-metallic doped VPOs catalysts in H_2/Ar stream. The temperature of peak maxima, total amount of oxygen removed in each peak and the derived reduction activation energy data of GdCe doped VPOs catalysts are summarised in Table 4.3.

Figure 4.3 shows that all of the GdCe doped VPOs catalysts exhibited two peak maxima. The existence of two kinetically different reduction peaks suggested the possibility of two different oxygen species were involved in reduction of H_2. The first peak maximum, within the temperature range of 774-799 K, corresponded to the reduction of oxygen (O^{2-}) species from V^{5+} phase whereas the second peak maximum, from the higher temperature range of 993-1014 K, was related to the removal of lattice oxygen (O^-) associated to V^{4+} phase. A similar phenomenon has also been reported by Abon et al. (2001). The second peak maxima, being the major peak between the two, indicated that V^{4+} was the predominant species in the catalyst as established in redox titration analyses. There was a significant shift in the reduction temperatures corresponding to the second peak maxima for the GdCe doped VPOs catalysts. For Gd1Ce5, the reduction temperature was lowered by approximately 20 K compared to Gd1Ce1 and Gd1Ce3 catalysts. This showed that the increasing amount of Ce dopant to 5.0 mol% has positive effect on the ease of oxygen reducibility from the VPOs catalysts, which would translate to higher catalytic activity.

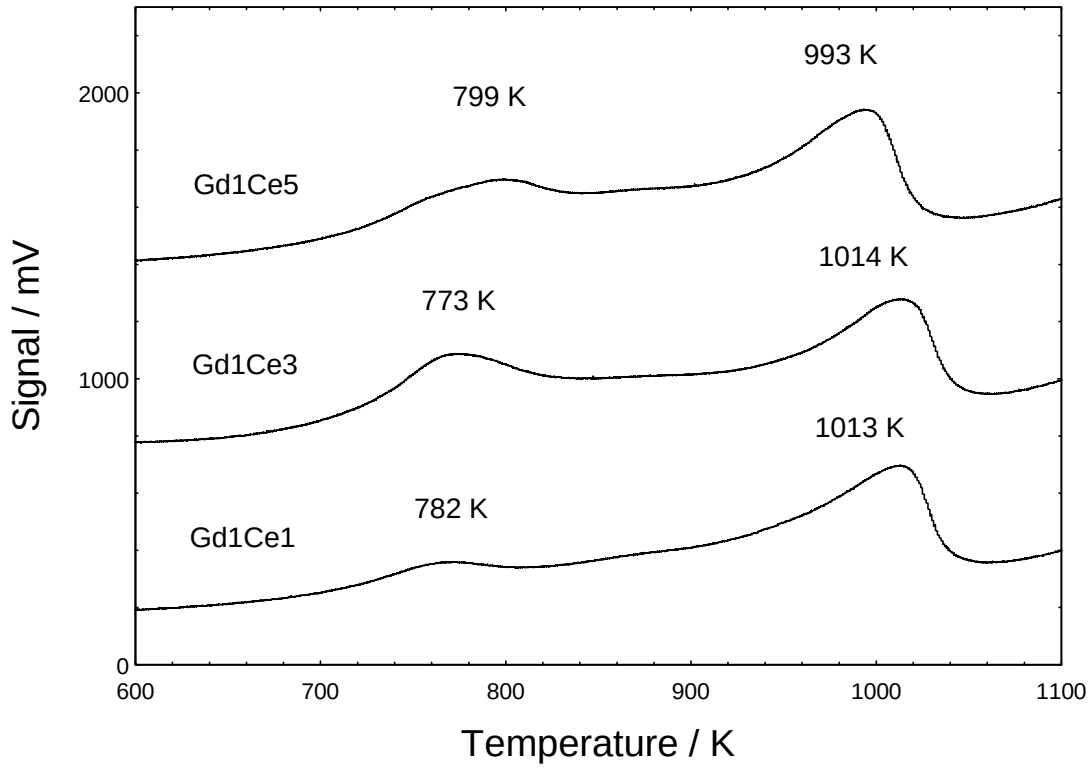

Figure 4.3: TPR in H_2 Profiles of GdCe Doped VPOs Catalysts

The amount of oxygen removed from both peaks of Gd1Ce1 were found to be 6.835 $\times 10^{20}$ and 1.392 $\times 10^{21}$ atom g^{-1}, respectively. As the mol% of Ce increased in the VPOs catalysts, the amount of oxygen atoms removed were also increased for both peaks maxima in Gd1Ce3 at 8.794 $\times 10^{20}$ and 1.459 $\times 10^{21}$ atom g^{-1}, and in Gd1Ce5 at 1.022 $\times 10^{21}$ and 1.579 $\times 10^{21}$ atom g^{-1}, respectively. In terms of total amount of oxygen removed for both peak maxima, the total amount removed for undoped bulk VPOs-R8 catalyst was 2.249 $\times 10^{21}$ atom g^{-1}, which was higher than 2.076 $\times 10^{21}$ atom g^{-1} for Gd1Ce1. With subsequent addition of higher concentration of Ce, Gd1Ce3 and Gd1Ce5 produced higher total amount of oxygen atoms removed than the bulk catalyst, at 2.338 $\times 10^{21}$ and 2.601 $\times 10^{21}$ atom g^{-1}, respectively.

Table 4.3: Total Amount of Oxygen Atoms Removed and Values of Reduction Activation Energies by Reduction in H_2 for the Bulk and GdCe Doped VPOs Catalysts

Catalyst	Peak	T_{max} (K)	Reduction activation energy, Er[a] (kJ mol^{-1})	Oxygen atom removed (mol g^{-1})	Oxygen atom removed (atom g^{-1})
VPOs-R8	1	744	124.4	3.530×10^{-4}	2.126×10^{20}
	2	1005	168.1	3.380×10^{-3}	2.036×10^{21}
	Total			3.733×10^{-3}	2.249×10^{21}
Gd1Ce1	1	782	130.8	1.136×10^{-3}	6.835×10^{20}
	2	1013	169.4	2.313×10^{-3}	1.392×10^{21}
	Total			3.449×10^{-3}	2.076×10^{21}
Gd1Ce3	1	774	129.4	1.461×10^{-3}	8.794×10^{20}
	2	1014	169.5	2.424×10^{-3}	1.459×10^{21}
	Total			3.885×10^{-3}	2.338×10^{21}
Gd1Ce5	1	799	133.6	1.698×10^{-3}	1.022×10^{21}
	2	993	166.0	2.623×10^{-3}	1.579×10^{21}
	Total			4.321×10^{-3}	2.601×10^{21}

[a]Values of activation energies are obtained from the modified version of Redhead equation, $\frac{E_r}{RT_m^{\,2}} = \left(\frac{A_r}{\beta}\right)[H_2]_m \exp\left(\frac{E_r}{RT_m}\right)$

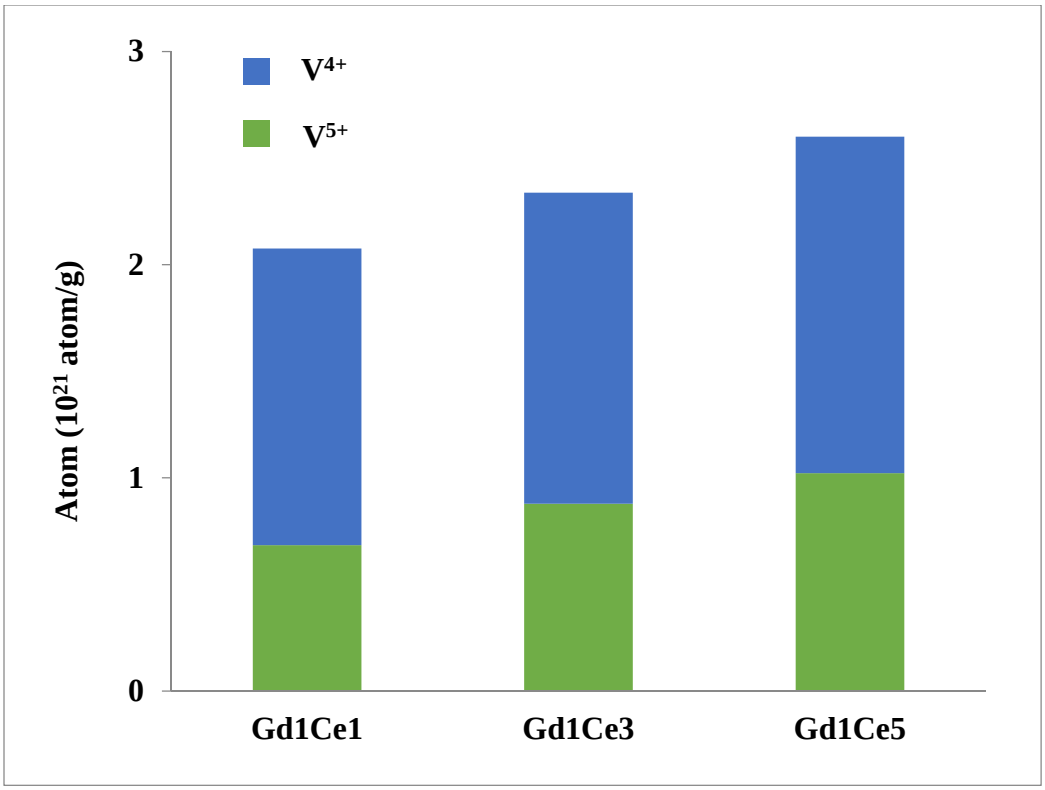

Figure 4.4: Amount of Oxygen Atoms Removed from V^{4+} and V^{5+} Phases for GdCe Doped VPOs Catalysts

TPR in H_2 results highlighted the promotional effect Ce dopant in oxygen reducibility in both V^{4+} and V^{5+} phases, thus resulting in an overall improvement in both activity and selectivity of the VPOs catalyst. By comparing the incremental trend of the results for BET and TPR analyses, a linear relationship can be drawn between the specific surface area of the catalysts and total amount of oxygen atoms removed from the catalysts with more mol% of Ce added. This pattern was also reported by Rownaghi et al. (2009) whereby the precursor impregnation by Ce alone resulted in significantly higher total amount of oxygen removed as compared to undoped VPO catalyst prepared using dihydrate method.

4.1.5 Series 1: Catalytic Oxidation of *n*-Butane Analyses

The catalytic performance of the GdCe doped VPOs catalysts for *n*-butane oxidation to maleic anhydride (MA) were tested at 673 K with GHSV = 2400 h^{-1}. Catalytic performances data derived from the analyses are listed in Table 4.4.

Table 4.4: Catalytic Performances of Bulk and GdCe Doped VPOs Catalysts

Catalyst	*n*-Butane conversion (%)	Product selectivity (%)		
		MA	CO	CO_2
VPOs-R8	20	67	1	32
Gd1Ce1	17	68	0	32
Gd1Ce3	25	70	0	30
Gd1Ce5	25	74	0	26

The percentage of *n*-butane conversion for Gd1Ce1, Gd1Ce3 and Gd1Ce5 were 17%, 25% and 25% respectively. It could be noticed that, with further addition of Ce, the activity of the VPOs catalyst improved markedly by 47%. The product selectivity were also increased from 68%, 70% and 74% for Gd1Ce1, Gd1Ce3 and Gd1Ce5 respectively. The selectivity percentages of the bi-metallic doped catalysts in this series were higher than the reported value of 65% for the commercial BASF-Petronas VPO catalyst. The findings on selectivity of GdCe doped catalysts were consistent with the outcome obtained by Shen et al. (2002) on Ce-Fe promoted VPO catalysts. They had also proposed that Ce led to improvement of redox performance

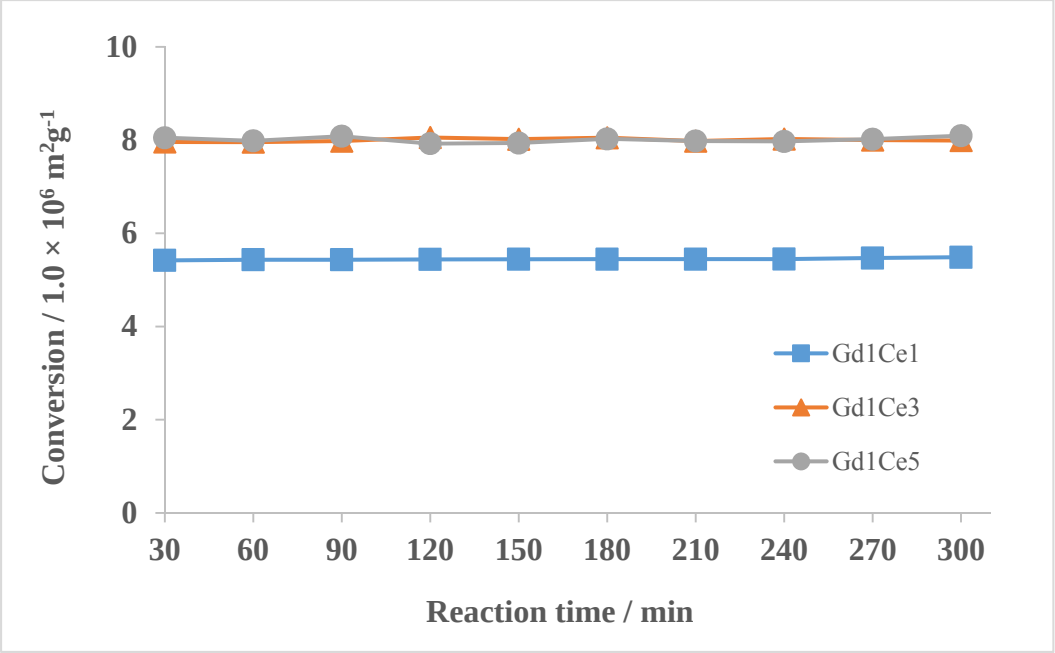

Figure 4.5: Conversion of *n*-Butane against Reaction Time for GdCe Doped VPOs Catalysts

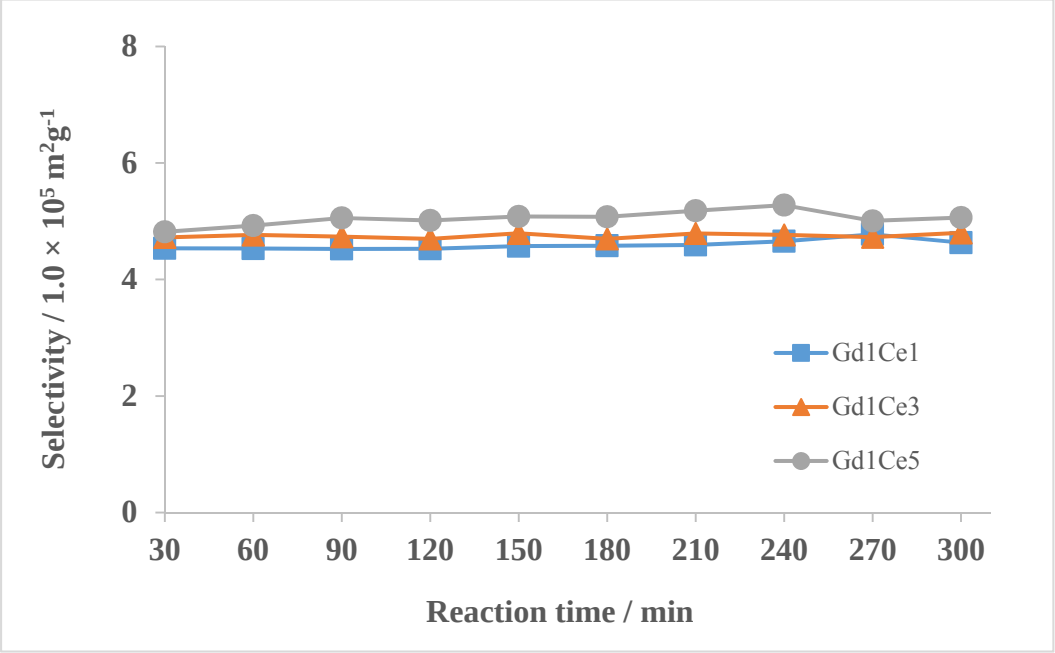

Figure 4.6: Selectivity to Maleic Anhydride against Reaction Time for GdCe Doped VPOs Catalysts

of the catalyst and formation of highly selective oxygen species for MA formation. Conversion of n-butane and selectivity to maleic anhydride against reaction time for the GdCe doped catalysts are shown in Figures 4.5 and 4.6 respectively.

In comparison to the catalytic performances of the bulk VPOs catalyst, Gd1Ce3 and Gd1Ce5 exhibited higher percentages in both *n*-butane conversion and selectivity to MA. All of the GdCe doped catalysts were considered to have performed better than the undoped bulk catalyst, with the exception of Gd1Ce1, which yielded slightly lower conversion than the bulk catalyst. The α_{II}-$VOPO_4$ phase, detected in all GdCe catalysts via XRD, has been shown to promote the *n*-butane conversion and selectivity of MA. With the increasing availability of the amorphous V^{5+} phase, due to increment in concentration of Gd and Ce, all of the GdCe catalysts exhibited higher product selectivity than the bulk VPOs catalyst.

The catalytic performance results were also in agreement with the TPR analyses due to the increased number of oxygen atoms removed for the GdCe doped VPOs catalysts. It can also be suggested that the change in nature of the active sites, such as the availability of more vanadyl group for activation of *n*-butane as reflected in XRD studies, played an important part in improving the activity of the GdCe bi-metallic doped catalysts. These findings demonstrated that the addition of Gd and Ce dopants improved the overall performance of the catalysts in this series of study.

4.1.6 Series 1: Conclusion

In the first series of this study, it was found that the synergistic effect, from the combination of Gd and Ce, played a direct role in inducing the formation of α_{II}-$VOPO_4$, V^{5+} phase. Addition of more mol% of Ce have also led to increase in specific surface area with more functional vanadyl group as well as high reducibility and selective oxygen species. In conclusion, these features in GdCe bi-metallic doped catalysts translated to increase in conversion percentage of *n*-butane and, higher selectivity to MA compared to the commercial VPO catalyst. Therefore, for the second series of this study, La will be added together with Ce in different combination percentages to synthesise LaCe doped VPOs catalysts with the aim to improve on the conversion of *n*-butane and investigate the synergistic effect of La and Ce on the performance of VPOs catalyst.

4.2 Series 2: Effect of La and Ce Bi-metallic dopants on the Physico-chemical and Catalytic Properties of Vanadyl Pyrophosphate Catalysts via Sesquihydrate Route

In the second series of this study, the vanadyl pyrophosphate (VPOs) catalysts were prepared via the sesquihydrate route with La and Ce dopants added in different mol percentages. The activated catalysts were denoted as LaXCeY (X = 1, Y = 1, 3, 5 mol%), with La1Ce1, La1Ce3 and La1Ce5 being synthesised. The effect of different combination percentages of La and Ce dopants on the physico-chemical, reactivity and catalytic properties of the VPOs catalysts will be studied. Bulk VPOs-R8, prepared by Leong et al. (2012), was designated as control sample and its experimental data were used as comparison in all analyses in this series of study.

4.2.1 Series 2: XRD Analyses

According to the patterns derived from the XRD analyses, Figure 4.7 also displayed three intense reflection peaks at 2θ = 22.8º, 28.4 º and 29.3º, which corresponded to (0 2 0), (2 0 4) and (2 2 1) planes respectively for the LaCe bi-metallic doped VPOs catalysts (JCPDS File No. 34-1381). These peaks corresponded to the crystalline V^{4+}, $(VO)_2P_2O_7$ phase were deemed to be for the activity of the VPOs catalysts (Haber et al. 1997).

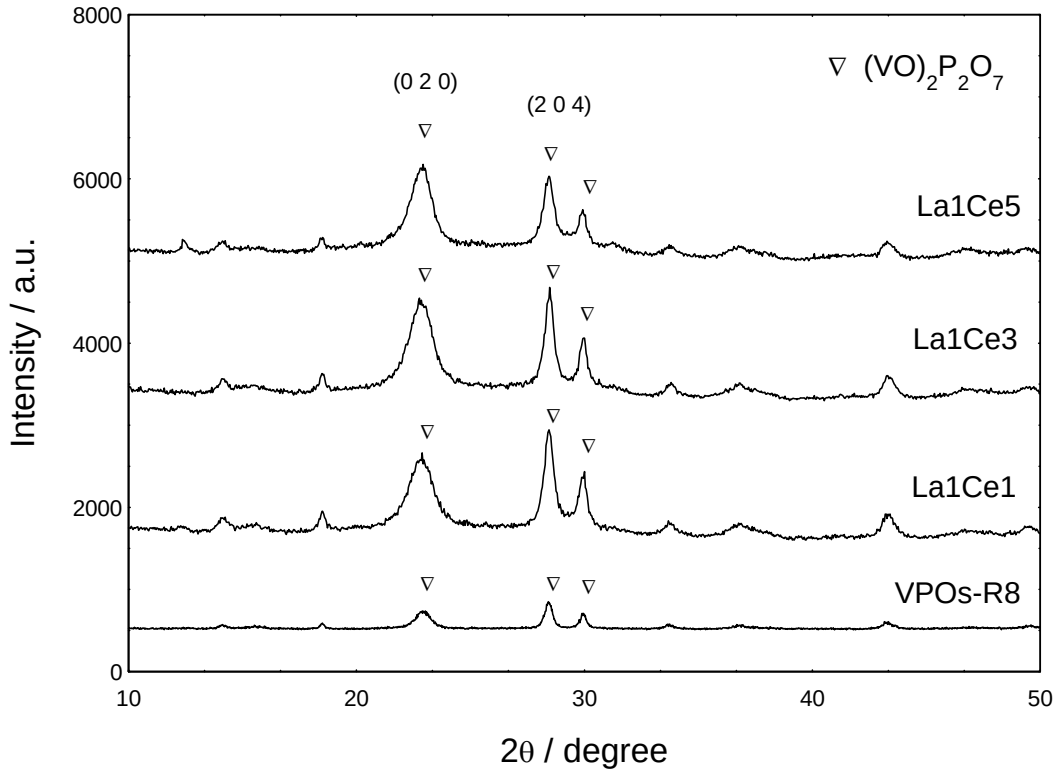

Figure 4.7: XRD Patterns for Bulk and LaCe Doped VPOs Catalysts

Crystallite sizes were calculated from the full-width half maximum (FWHM) values and listed in Table 4.5. For the LaCe doped catalysts series, the crystallite size at (0 2 0) plane increased from 61.64 Å, 62.90 Å to 70.28 Å for La1Ce1, La1Ce3 and La1Ce5, respectively. Similarly to the GdCe series, the crystallite size along the (2 0 4) reflection plane decreased with the addition of higher concentration of Ce into the catalyst system. This pattern further proved that Ce has an effect on the morphology of VPOs catalyst. In overall, the crystallite sizes of the LaCe doped catalysts are larger than the GdCe doped catalysts along both (0 2 0) and (2 0 4) planes. It could be deduced that the addition of La promoted the increase of crystallite size.

Table 4.5: XRD Data of Bulk and LaCe Doped VPOs Catalysts

Catalyst	Line width[a] (°)		Crystallite size[b] (Å)		I_{020}/I_{204}[c]
	(0 2 0)	(2 0 4)	(0 2 0)	(2 0 4)	
VPOs-R8	0.7400	0.3869	108.28	209.37	0.52
La1Ce1	1.2997	0.6298	61.64	128.63	0.48
La1Ce3	1.2763	0.6505	62.90	124.54	0.51
La1Ce5	1.1398	0.6798	70.28	119.16	0.59

[a]FWHM of (0 2 0) and (2 0 4) reflection planes
[b]Crystallite size by means of Scherrer equation
[c]Intensity ratio between (0 2 0) and (2 0 4) reflection planes

It could also be observed that the peaks related to amorphous V^{5+} phase were not found. This could be due to the reason that the amount of V^{5+} was below the detection limit of the XRD equipment. However, according to Cavani et al. (2000), there might be as high as up to 20% of $VOPO_4$, V^{5+} phase in addition of $(VO)_2P_2O_7$ could be found in the VPO catalyst without being detected by the XRD. As the V^{5+} phase is known to be responsible in selectivity to MA, this revelation will be explained further in the catalytic performances test for this series of study. The ratio between the intensity of (0 2 0) and (2 0 4) plane also increased due the increase in the relative exposure of vanadyl group along the (0 2 0) plane, which translated to enhancement of catalytic activity (Haber et al. 1997). Likewise with GdCe series, the crystallite sizes of the LaCe doped catalysts were significantly lower than the bulk VPOs-R8 catalyst along both (0 2 0) and (2 0 4) planes.

4.2.2 Series 2: BET Surface Area and Chemical Analyses

Results from BET surface area measurement, ICP-OES, EDX and redox titration for the LaCe doped VPOs catalysts are tabulated in Table 4.6.

Table 4.6: Specific Surface Area, Chemical Compositions, Average Oxidation Numbers and Percentages of V^{4+} and V^{5+} Oxidation States Present in Bulk and LaCe Doped VPOs Catalysts

Catalyst	Surface area (m^2g^{-1})	P/V ratio (ICP-OES)	P/V ratio (EDX)	Average oxidation number of vanadium		
				V^{4+} (%)	V^{5+} (%)	V_{AV}
VPOs-R8	19.00	1.03	1.12	95.81	4.19	4.0419
La1Ce1	17.50	1.25	1.24	93.33	6.67	4.0667
La1Ce3	17.23	1.25	1.32	91.53	8.47	4.0847
La1Ce5	18.32	1.23	1.29	90.98	9.02	4.0902

From the data acquired from BET measurements, it was shown that the specific surface area was not markedly improved with the higher concentration of cerium. However, compared to GdCe doped catalysts, VPOs catalysts doped with different combination percentages of La and Ce were found to exhibit marginally higher specific area of 17.50, 17.23 and 18.32 m^2g^{-1} for La1Ce1, La1Ce3 and La1Ce5 doped catalysts, respectively. It could be reasoned that La combined better

with Ce than Gd, in terms of inducing a less bulky structure of the catalyst and thus, promotion of specific surface area of the VPOs catalysts. The disparity in synergistic effect between LaCe and GdCe continued to be observed in TPR and catalytic test results.

ICP-OES data revealed that the stoichiometric P/V atomic ratio for La1Ce1, La1Ce3 and La1Ce3 were 1.25, 1.25 and 1.23 respectively. According to the EDX analyses, it was shown that the P/V atomic ratio ranged from 1.24 to 1.32. The P/V atomic ratio results of the LaCe doped VPOs catalysts were slightly higher than the optimal range (P/V $\geq$ 1.0) for producing of $(VO)_2P_2O_7$ phase (Centi, 1993). P/V atomic ratio was not markedly affected by the presence of increasing concentration of Ce. Still, the addition La and Ce dopants resulted to greater stabilisation of the V^{4+} phase on the VPOs catalysts and would lead to higher activity, compared to the bulk catalyst. This finding was observed in the *n*-butane conversion result from the catalytic tests.

From the redox titration results, the average oxidation number of vanadium, V_{AV} for La1Ce1, La1Ce3 and La1Ce5 were determined as 4.0667, 4.0847 and 4.0902 respectively. The decrease in V_{AV} of the LaCe doped catalysts, compared to GdCe doped catalysts, was due to the lack of significant amount of V^{5+} species as illustrated in the XRD patterns in Figure 4.7. In comparison to the effect from the bi-metallic combination of Gd and Ce on the V_{AV} state, the existence of 1 mol% of La together with Ce has somewhat resulted in retardation of the V^{5+} phase and

would lead to a less bulky structure, which was apparent in the SEM micrographs. This revelation was also reflected in the reduction in product selectivity for the LaCe doped catalysts from the catalyst performance test.

4.2.3 Series 2: SEM Analyses

Surface morphologies of LaCe doped VPOs catalysts were obtained using scanning electron microscopy (SEM). The retrieved micrographs are shown in Figure 4.8(a)-(c). LaCe doped catalysts also exhibited the same secondary structure of plate-like crystals in different sizes of rosette-shaped agglomerates alike the GdCe doped catalysts. However, the rosette crystals of the LaCe catalysts were thinner and in smaller uniformed size compared to the GdCe catalysts.

From the SEM observations, the addition of La allowed the catalyst to fold into less bulky layered structure that was exposed to the (1 0 0) reflection plane (Kiely et al. 1995). This observation conformed to the higher specific surface area detected in BET measurement data. It could be pointed that, with the increasing mol% of Ce added together with La, the morphology of the VPOs catalyst were enhanced by the synergistic effect from the La and Ce combination, leading to higher *n*-butane conversion to MA compared to the GdCe series. Ultimately, this finding was reflected in the catalytic performance results.

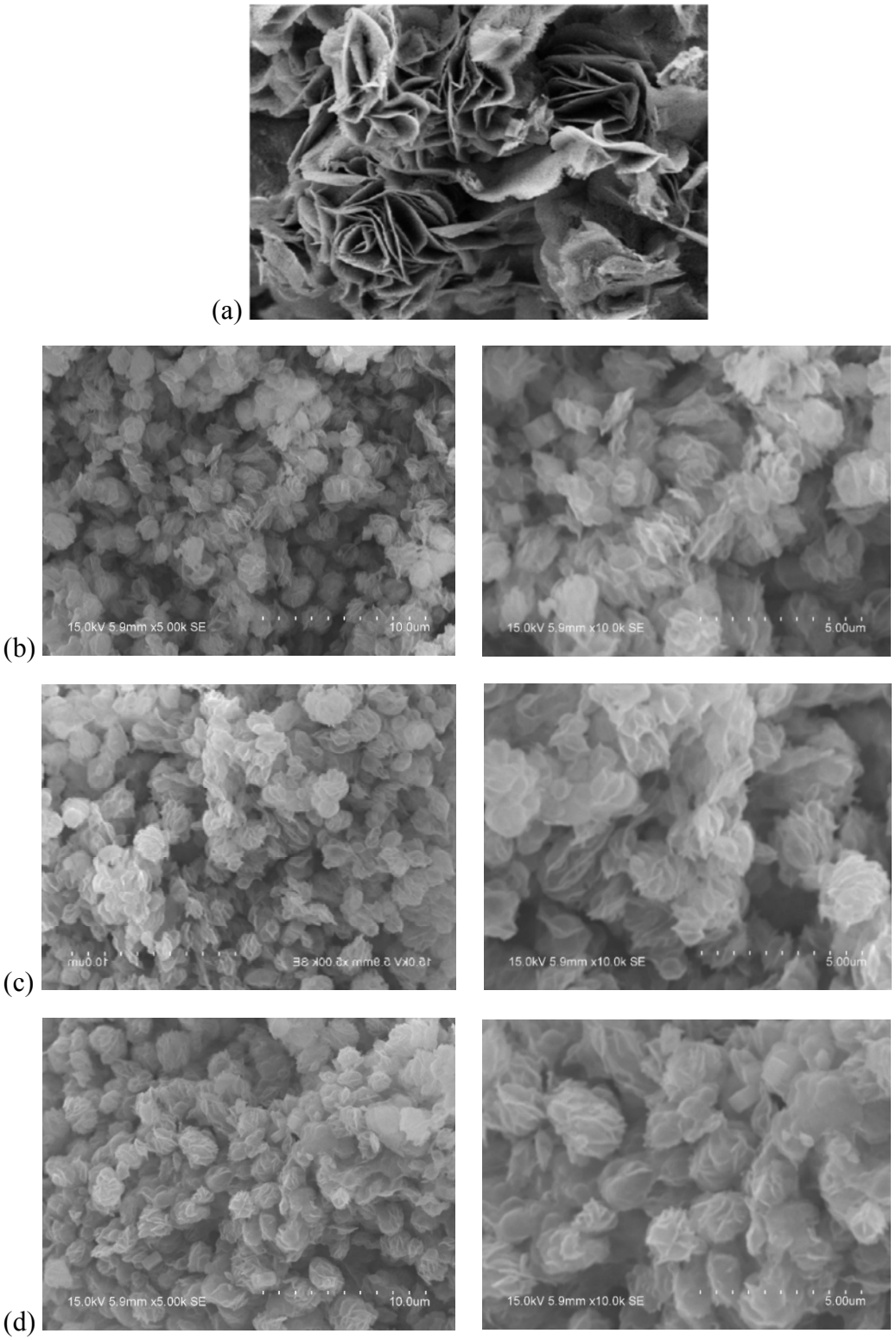

Figure 4.8: SEM Micrographs of (a) VPOs-R8 (b) La1Ce1 (c) La1Ce3 and (d) La1Ce5 Catalysts (Magnification × 5000 and 10000)

4.2.4 Series 2: TPR in H_2 Analyses

Figure 4.9 shows the TPR profiles for LaCe doped VPOs catalysts in H_2/Ar stream. The temperature of peak maxima, total amount of oxygen removed in each peak and the derived reduction activation energy data of LaCe doped VPOs catalysts are tabulated in Table 4.7.

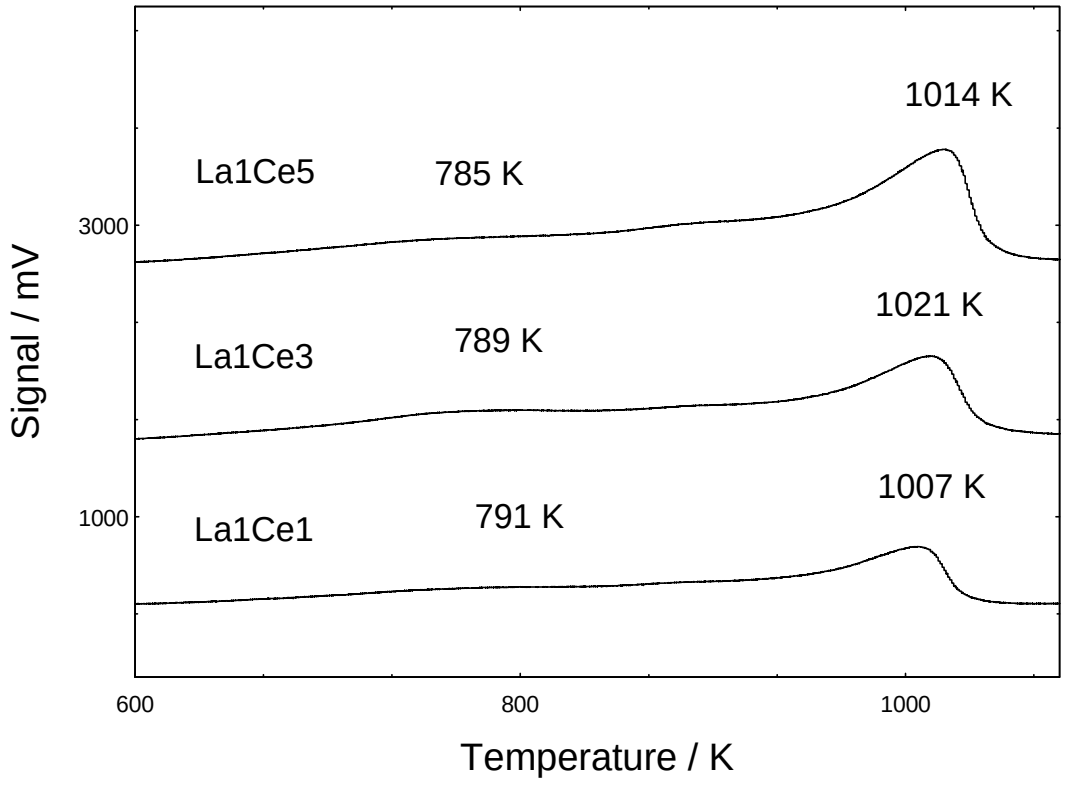

Figure 4.9: TPR in H_2 Profiles of LaCe Doped VPOs Catalysts

From the observation on the TPR profile in Figure 4.9, it was revealed that LaCe doped VPOs catalysts exhibited two maximum peaks, which was similar to the GdCe doped catalysts. Therefore, it also mean that there are two different oxygen species that were involved in consumption of H_2 of the catalysts in this series of study. The first and second peaks corresponded to the removal of lattice oxygen from the selective V^{5+} (O^{2-}) and active V^{4+}(O^{-}) phases, respectively.

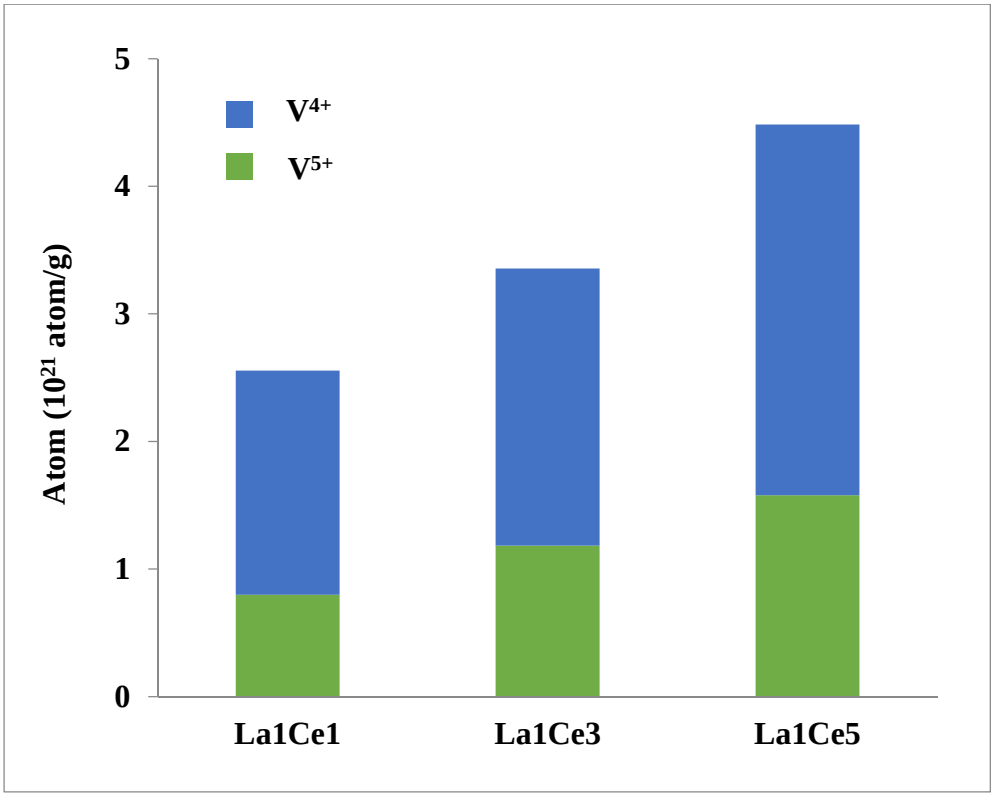

Figure 4.10: Amount of Oxygen Atoms Removed from V^{4+} and V^{5+} Phases for LaCe Doped VPOs Catalysts

Table 4.7: Total Amount of Oxygen Atoms Removed and Values of Reduction Activation Energies by Reduction in H_2 for the Bulk and LaCe Doped VPOs Catalysts

Catalyst	Peak	T_{max} (K)	Reduction activation energy, Er[a] (kJ mol^{-1})	Oxygen atom removed (mol g^{-1})	Oxygen atom removed (atom g^{-1})
VPOs-R8	1	744	124.4	3.530×10^{-4}	2.126×10^{20}
	2	1005	168.1	3.380×10^{-3}	2.036×10^{21}
	Total			3.733×10^{-3}	2.249×10^{21}
La1Ce1	1	791	132.3	1.326×10^{-3}	7.982×10^{20}
	2	1007	168.4	2.920×10^{-3}	1.758×10^{21}
	Total			4.246×10^{-3}	2.556×10^{21}
La1Ce3	1	789	131.9	1.968×10^{-3}	1.184×10^{21}
	2	1021	170.7	3.607×10^{-3}	2.172×10^{21}
	Total			5.575×10^{-3}	3.356×10^{21}
La1Ce5	1	785	131.3	2.623×10^{-3}	1.579×10^{21}
	2	1014	169.5	4.825×10^{-3}	2.905×10^{21}
	Total			7.448×10^{-3}	4.484×10^{21}

[a]Values of activation energies are obtained from the modified version of Redhead equation, $\frac{E_r}{RT_m^{\,2}} = \left(\frac{A_r}{\beta}\right)[H_2]_m \exp\left(\frac{E_r}{RT_m}\right)$

The total amount of oxygen removed from both peaks of La1Ce1 were calculated to be 7.982×10^{20} and 1.758×10^{21} atom g^{-1} respectively. As the mol% of Ce increased in the VPOs catalysts, the amount of oxygen atoms removed were also increased for both peaks maxima in La1Ce3 at 1.184×10^{21} and 2.172×10^{21}, and in La1Ce5 at 1.579×10^{21} and 2.905×10^{21} atom g^{-1}, respectively. In terms of total of oxygen removed for both peak maxima, the amount removed for all of the LaCe doped catalysts were higher than the bulk catalyst. Up to 50% increase in total number of oxygen atoms removed was recorded for La1Ce5.

In overall, it can be deduced that, with the increment of mol% of Ce, amount of oxygen removed also increased. Gd has shown to have an inhibitory effect to the reducibility of the VPOs catalysts within the range of study. Once La was paired with Ce as bi-metallic dopant, the amount of oxygen atoms removed were significantly higher than the GdCe doped catalysts. This finding was supported by the BET measurement, SEM and chemical analyses results. It can be construed that the LaCe combination have better synergistic effect on the VPOs catalysts compared to the GdCe combination. This effect was demonstrated further in the increase in *n*-butane conversion to MA.

4.2.5 Series 2: Catalytic Oxidation of *n*-Butane Analyses

The catalytic performance of the LaCe doped VPOs catalysts for *n*-butane oxidation to maleic anhydride (MA) were tested at 673 K with GHSV = 2400 h^{-1}. Catalytic performance data produced from the analyses are shown in Table 4.8.

Table 4.8: Catalytic Performances of Bulk and LaCe Doped VPOs Catalysts

Catalyst	*n*-Butane conversion (%)	Product selectivity (%)		
		MA	CO	CO_2
VPOs-R8	20	67	1	32
La1Ce1	29	62	0	38
La1Ce3	37	63	0	37
La1Ce5	41	62	0	38

The *n*-butane conversion for La1Ce1, La1Ce3 and La1Ce5 were 29%, 37% and 41%, respectively. Though, the product selectivity remained within the range of 62-63%, which was still comparable to the 65% selectivity for the commercial BASF-Petronas VPO catalyst prepared using conventional organic method. As a measure of the performance of the LaCe doped catalysts, the catalytic performance data of this series were compared with the data derived from the bulk VPOs-R8 catalyst prepared by Leong et al. (2012) via sesquihydrate route. All of the LaCe doped bi-metallic VPOs catalysts exhibited higher percentages of *n*-butane conversion with slightly lower selectivity to MA. Conversion of n-butane and

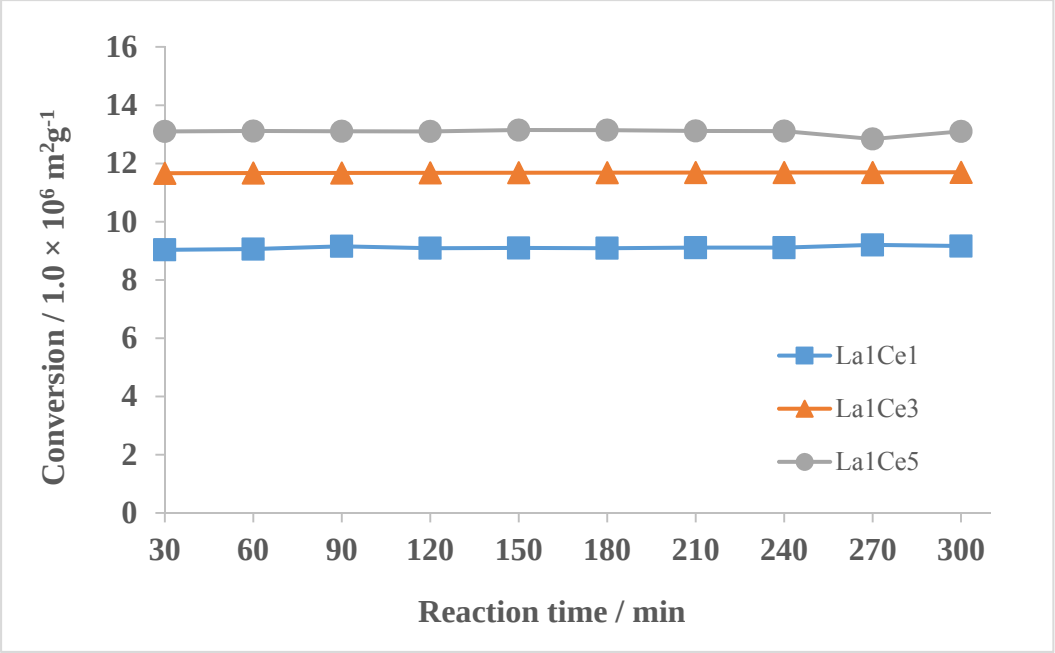

Figure 4.11: Conversion of *n*-Butane against Reaction Time for LaCe Doped VPOs Catalysts

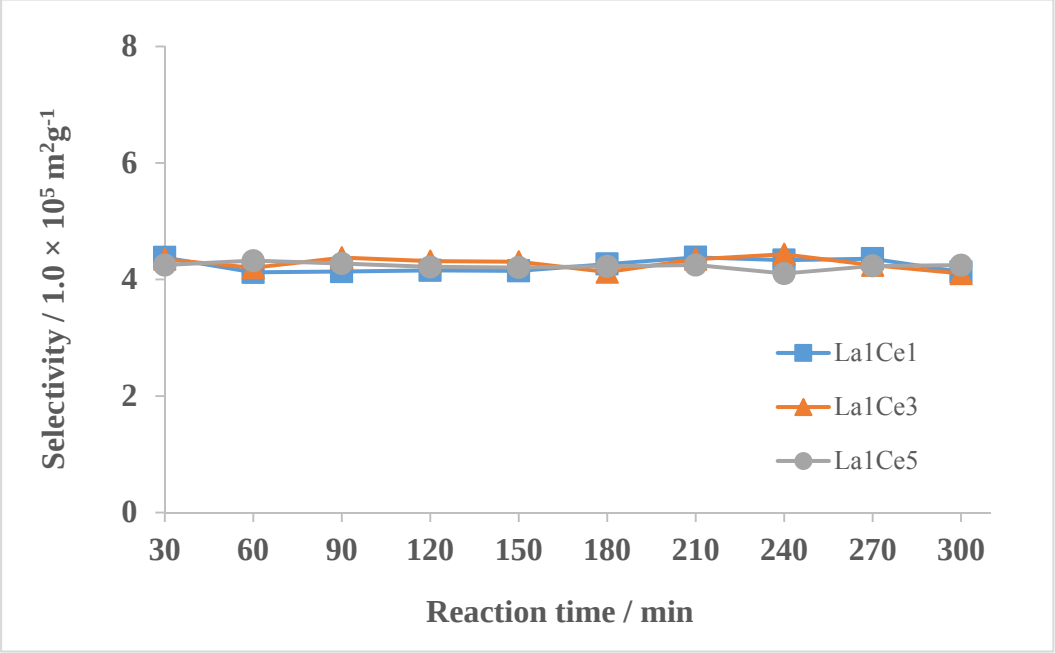

Figure 4.12: Selectivity to Maleic Anhydride against Reaction Time for LaCe Doped VPOs Catalysts

selectivity to maleic anhydride against reaction time for the LaCe doped catalysts are shown in Figures 4.11 and 4.12 respectively.

As observed in the catalytic performance of the GdCe doped catalyst in the first series, it was noticeable that with further addition of Ce, the activity of the VPOs catalyst was improved. The synergistic effect from the combination of La and Ce was shown to induce higher *n*-butane conversion, albeit resulted to a small reduction in selectivity to MA, which could be attributed to the lesser amount of V^{5+} phase compared to the GdCe series. These results were in agreement with the observations on XRD, BET, chemical analyses and TPR in H_2 results.

4.2.6 Series 2: Conclusion

In the second series of this study, it was shown that the catalytic performances of the VPOs catalyst improved with the addition of La and Ce dopants. Ce played a direct role in inducing the promotion of crystalline $(VO)_2P_2O_7$, V^{4+} phase, increase in specific surface area and in ease of reducibility of oxygen. Notwithstanding the lower specific surface area and lesser V^{4+} phase than the bulk VPOs-R8 catalyst, factors such as higher exposure of vanadyl group along (0 2 0) plane and stabilisation of V^{4+} phase have resulted to higher activity for the LaCe doped catalysts. In conclusion, these features in LaCe bi-metallic doped catalysts led to higher conversion percentage of *n*-butane as compared to bulk VPOs-R8 and comparable selectivity to MA to the commercial VPO catalyst.

CHAPTER 5

CONCLUSION

Bi-metallic GdCe and LaCe doped VPOs catalysts were synthesised successfully using 1-butanol as reducing agent prepared via sesquihyrdate route. The effect of mole percentages of bi-metallic GdCe and LaCe dopants on VPO catalysts, was also examined successfully using various physical, chemical and reactivity tests. Both GdCe and LaCe bi-metallic doped VPOs catalysts exhibited three main reflection peaks of $(VO)_2P_2O_7$ phase 2θ = 22.8º, 28.4 º and 29.0º that corresponded to (0 2 0), (2 0 4) and (2 2 1) planes respectively. GdCe doped catalysts contained additional distinct α_{II}-$VOPO_4$, V^{5+} phase but the amorphous phase was not detected in the LaCe doped catalysts. GdCe doped catalysts showed lower specific surface area compared to the LaCe counterpart, with La1Ce5 exhibited the highest specific surface area of 18.32 m^2g^{-1}. From the SEM micrographs, surface morphologies of the GdCe doped VPOs catalysts displayed rough and plate-like crystals whereas, thin uniform-sized rosette clusters were observed in LaCe doped catalysts which would lead to higher surface area. Chemical analyses showed the presence of V^{5+} phases in GdCe doped catalysts, which corresponded to higher selectivity to MA. TPR in H_2 profile revealed that two peak maxima which corresponded to the oxygen removal from $V^{5+}(O^{2-})$ and $V^{4+}(O^{-})$ phases for all of the doped catalysts. La1Ce5 displayed the highest amount of oxygen atoms being removed with the total of 4.484×10^{21} atom g^{-1}. Catalytic

tests also showed that La1Ce5 has the highest *n*-butane conversion of 41% with a relatively high selectivity of 62%. The selectivity was comparable to commercial VPO catalyst. In summary, it can be concluded that La1Ce5 is the best performing catalyst within the range of study of the GdCe and LaCe series.

Suggestions for future study:

i. Catalyst support, such as titania or alumina, to be applied in the bi-metallic doped VPOs catalysts with the view to improve further on the catalytic performance.

ii. Concentration of Ce dopant to be increased to possibly synthesise VPOs catalyst that will lead to higher conversion of *n*-butane to MA.

iii. Different characterisation techniques, such as electron spin resonance (ESR) spectroscopy, extended X-ray absorption fine structure (EXAFS) and X-ray absorption near edge structure (XANES), could be employed to provide more insight on the nature of the VPOs catalyst.

REFERENCES

Book:

Anastas, P.T. and Warner J.C., 1998. *Green chemistry: theory and practice*. New York: Oxford University Press, pp. 2-135.

Bond G.C., 1987. *Heterogeneous catalysis: principles and applications*. 2nd ed. New York: Oxford University Press, pp. 2-90.

Centi G., Cavani F. and Trifiro F., 2001. *Selective Oxidation by Heterogeneous Catalysis*. New York: Springer, pp. 37-38.

Chemical Week, 2005. May 18, p. 26.

Chorkendorff I. and Niemantsverdriet J.W., 2007. *Concepts of Modern Catalysis and Kinetics*. 2nd Edition, Wiley-VCH, pp. 2-167.

Elschenbroich C. and Salzer A., 1992. *Organometallics: A Concise Introduction*. 2nd Edition, Wiley-VCH, p. 758.

Fadoni, M. and Lucarelli, L., 1998. *Temperature programmed desorption, reduction, oxidation and flow chemisorption for the characterisation of heterogeneous catalysts. Theoretical aspects, instrumentation and applications*. Milan: ThermoFinnigan, pp. 3 – 44.

Hartley F.R., 1985. *Supported metal complexes: A New Generation of Catalysts*. Holland: Springer, p. 235.

Kolasinski K.W., 2008. *Surface Science: Foundation of Catalysis and Nanoscience*, 2nd ed, London: Wiley, p. 508.

Kurosawa H. and Yamamoto A., 2003. *Current Methods in Inorganic Chemistry Vol. 3: Fundamentals of Molecular Catalysis*. Amsterdam: Elsevier, p. 1.

Lohbeck K., Haferkorn H., Fuhrmann W. and Fedtke N., 2012. *Maleic and Fumaric Acids. Ullmann's Encyclopedia of Industrial Chemistry*, Wiley-VCH Verlag GmbH & Co. KGaA, pp. 145-155.

Maleic Anhydride Market Analysis and Segment Forecasts to 2020, 2014. Grand View Research Inc., pp. 9-26.

Taufiq-Yap Y.H., 2009. *Catalysis for a sustainable world*, Universiti Putra Press, p. 1.

Trivedi, B.C. and Culbertson B.M., 1982. *Maleic anhydride*. New York: Plenum Press, pp. 17-40.

Yates, J.G. and Lettieri, P., 2016. *Introduction. In Fluidized-Bed Reactors: Processes and Operating Conditions*. Springer International Publishing, pp. 1-21.

Journal:

Abdelouahab F.B., Olier R., Ziyad M. and Volta J.C., 1995. The role of Fe and Co dopants during the $VO(HPO_4)\cdot 0.5H_2O$ precursor of the vanadium phosphorus catalyst as studied by in situ laser Raman spectroscopy. *Journal of Catal*ysis, 157, pp. 687-697.

Abon M. and Volta J.C., 1997. Vanadium phosphorus oxides for *n*-butane oxidation to maleic anhydride. *Applied Catalysis A*: *General*, 157, pp. 173-193.

Abon, M., Herrmann, J.M. and Volta, J.C., 2001. Correlation with the redox V^{5+}/V^{4+} ratio in vanadium phosphorus oxide catalysts for mild oxidation of *n*-butane to maleic anhydride. *Catalysis Today*, 71, pp. 121–128.

Ballarini, N., Cavani F., Cortelli C., Ligi S., Pierelli F., Trifiro F., Fumagalli C., Mazzoni G. and Monti T., 2006. VPO catalyst for *n*-butane oxidation to maleic anhydride: A goal achieved, or a still open challenge?, *Topics in Catalysis*, 38, pp. 1-3.

Bergeret G., David M., Broyer J.P. and Volta J.C., 1987. A contribution to the knowledge of the active sites of VPO catalysts for butane oxidation to maleic anhydride. *Catalysis Today*, 1, pp. 37-47.

Bergmann R.L. and Frisch N.W., 1966. Production of maleic anhydride by oxidation of *n*-butane. *US Patent 3293268*.

Bither Jr. T.A., 1984. Catalyst for vapor phase oxidation of *n*-butane to maleic anhydride. *US Patent US4442226*.

Bordes E. and Courtine P., 1979. Some selectivity criteria in mid oxidation catalysis: V-P-O phases in butane oxidation to maleic anhydride. *Journal of Catalysis*, 57, pp. 236-252.

Bordes E., 1987. Crystallochemistry of V-P-O phases and application to catalysis. *Catalysis Today*, 1, pp. 499-525.

Bordes E., 2001. Synergistic effects in selective oxidation catalysis: does phase cooperation result in site isolation? *Topics in Catalysis*, 1, pp. 131-136.

Bremer N.J. and Dria D.E., 1983. Preparation of mixed vanadium phosphorus oxide catalysts. *US Patent 4396535*.

Brunauer S., Emmett P.H. and Teller E., 1938. Adsorption of gases in multimolecular layers. *Journal of the American Chemical Society*, 60, pp. 309-319.

Cavani F., Centi G. and Trifiro F., 1984. The chemistry of catalysts based on vanadium-phosphorus oxides. Note IV: Catalytic behavior of catalysts prepared in organic medium in the oxidation of C_4 fraction. *Applied Catalysis*, 9, pp. 191-202.

Cavani F., Ligi S., Monti T., Pierelli F., Trifiro F., Albonetti S. and Mazzoni G., 2000. Relationship between structural/surface characteristics and reactivity in *n*-butane oxidation to maleic anhydride: The role of V^{3+} species. *Catalysis Today*, 61, pp. 203-210.

Cavani, F. and Trifiro, F., 1994. The characterisation of the surface properties of V-P-O catalysts by probe molecules. *Applied Catalysis A*, 195-221.

Cavani F. and Trifiro F., 1994b. Selective oxidations of C_4 paraffins. *Catalysis*, 11, The Royal Society of Chemistry, Cambridge, p. 246.

Centi G., Trifiro F., Ebner J.R. and Franchetti V.M., 1988. Mechanistic aspects of maleic anhydride synthesis from C4 hydrocarbons over phosphorus vanadium oxide. *Chemical Reviews*, 88, pp. 55-80.

Centi G., 1993. Vanadyl Pyrophosphate - A Critical Overview, *Catalysis Today*, 16, pp. 5-26.

Chen J., 2014. Homogeneous and heterogeneous catalysis: teachings of the thermal energy and power engineering course. *International Journal of Social, Behavioral, Educational, Economic, Business and Industrial Engineering*, 8, p. 1.

Cheng W. and Wang W., 1997. Effect of calcinations environment on the selective oxidation of *n*-butane to maleic anhydride over promoted and unpromoted VPO catalysts. *Applied Catalysis A: General*, 156, pp. 57-69.

Contractor R.M., 1991. Vapor phase catalytic oxidation of butane to maleic anhydride. *US Patent 5021588*.

de Souza Porto, M.F. and de Freitas, C.M., 1996. Major chemical accidents in industrializing countries; the socio-political amplification of risk. *Risk Analysis*, 16, pp. 19-29.

Dmuchovsky B., Freerks M.C., Pierron E.D., Munch R.H. and Zienty F.B., 1965. A study of the catalytic oxidation of benzene to maleic anhydride. *Journal of Catalysis*, 4, pp. 291-300

Felthouse T.R., Keppel R.A. and Schaefer J., 1997. Production of maleic anhydride using molybdenum-modified vanadium-phosphorus oxide catalysts. *US 5929256*.

Haber J., Zazhigalov V.A., Stoch J., Bogutskaya L.V. and Batcherikova I.V., 1997. Mechanochemistry: the activation method of VPO catalysts for *n*-butane partial oxidation. *Catalysis Today*, 33, pp. 39-47.

Heine, C., Hävecker, M., Trunschke, A., Schlögl, R. and Eichelbaum, M., 2015. The impact of steam on the electronic structure of the selective propane oxidation catalyst MoVTeNb oxide (orthorhombic M1 phase). *Physical Chemistry Chemical Physics*, 17(14), pp.8983-8993.

Hodnett B.K., Permanne P. and Delmon B., 1983. Influence of P/V ratio on the phase composition and catalytic activity of vanadium phosphate based catalysts. *Applied Catalysis*, 6, pp. 231-244.

Homma, T. and Kitaoka, T., 2014. Multiphase catalytic oxidation of alcohols over paper-structured catalysts with micrometer-size pores. *Applied Catalysis A: General*, 486, pp.201-209.

Horowitz H.S., Blackstone C.M., Sleight A.W. and Teufer G., 1988. V-P-O catalysts for oxidation of butane to maleic anhydride: Influence of $(VO)_2H_4P_2O_9$ precursor morphology on catalytic properties. *Applied Catalysis*, 38, pp. 193-210.

Hutchings G.J., 1991. Effect of promoters and reactant concentration on the selective oxidation of *n*-butane to maleic anhydride using vanadium phosphorus oxide catalysts. *Applied Catalysis*, 72, pp. 1-32.

Hutchings G.J., Sananes M.T., Sajip S., Kiely C.J., Burrows A., Ellison I.J. and Volta J.C., 1997. Improved method of preparation of vanadium phosphate catalysts, *Catalysis Today* 33, pp. 161-171.

Kiely C.J., Sajip S., Ellison I.J., Sananes M.T., Hutchings G.J. and Volta J.C., 1995. Electron microscopy studies of vanadium phosphorus oxide catalysts derived from $VOPO_4 \cdot 2H_2O$. *Catalysis Letters*, 33, pp. 357-368.

Kwon J.T. and Stanecki J.W., 1994. Stabilization of mixtures of maleic anhydride and acrylic acid during distillation, *US Patent US5319106*.

Leong L.K., Chin K.S. and Taufiq-Yap Y.H., 2011. The effect of Bi promoter on vanadium phosphate catalysts synthesized via sesquihydrate route. *Catalysis Today*, 164, pp. 341-346.

Leong L.K., Chin K.S. and Taufiq-Yap Y.H., 2012. Effect of varying reflux durations on the physico-chemical and catalytic performance of vanadium phosphate catalysts synthesized via vanadyl hydrogen phosphate sesquihydrate. *Applied Catalysis A: General*, 415-416, pp. 53-58.

Maki, A.W., 1991. The Exxon Valdez oil spill: initial environmental impact assessment. *Environmental Science and Technology*, 25, pp. 24-29.

Mallada R., Sajip S., Kiely C.J., Menendez M. and Santamaria J., 2000. Influence of the reaction atmosphere on the characteristics and performance of VPO catalysts. *Journal of Catalysis*, 196, pp. 1-7.

Matsuura I., Ishimura T. and Kimura N., 1995. Preparation and characterization of vanadyl hydrogen phosphate hydrates; $VO(HPO_4) \cdot 1.5H_2O$ and $VO(HPO_4) \cdot 0.5H_2O$. *Chemistry Letters*, 24, pp. 769-770.

Mizuno N., Hatayama H. and Misono M., 1997. One-pot synthesis of $VOHPO_4 \cdot 0.5H_2O$ with high growth of the (0 0 1) plane: An important catalyst precursor of $(VO)_2P_2O_7$. *Chemistry of Materials*, 9 (12), pp. 2697-2698.

Narayana K.V., Martin A., Lucke B., Belmans M., Boers F. and Deynse D.V., 2004. Preparation, solid-state characteristics, and catalytic properties of promoted vanadium phosphate materials. *Zeitschrift fur anorganische und allgemeine Chemie*, 631, pp. 25-30.

Niwa M. and Murakami Y., 1982. Reaction mechanism of ammoxidation of toluene IV. Oxidation state of vanadium oxide and its reactivity for toluene oxidation. *Journal of Catalysis*, 76(1), pp. 9-16.

Oliveira P.G Pd., Eon J.G., Chavant M., Riche A.S., Martin V., Caldarelli S. and Volta J.C., 2000. Modification of vanadium phosphorus oxides used for *n*-butane oxidation to maleic anhydride by interaction with niobium phosphate. *Catalysis Today*, 57, pp. 177-186.

Poli G., Resta I., Ruggeri O. and Trifiro F., 1981. The chemistry of catalysts based on vanadium-phosphorus oxides; Note II, the role of the method of preparation. *Applied Catalysis*, 1, pp. 395-404.

Qian Q., Zhang J., Cui M. and Han B., 2016. Synthesis of acetic acid via methanol hydrocarboxylation with CO_2 and H_2. *Nature Communications*, 7, pp. 1-7.

Romano, A., Di Giuliano, A., Gallucci, K., Foscolo, P.U., Cortelli, C., Gori, S. and Novelli, M., 2016. Simulation of an industrial turbulent fluidized bed reactor for *n*-butane partial oxidation to maleic anhydride. *Chemical Engineering Research and Design*, 114, pp.79-88.

Rownaghi A.A., Taufiq-Yap Y.H. and Rezaei F., 2009. Influence of rare-earth and bimetallic promoters on various VPO catalysts for partial oxidation of *n*-butane. *Catalysis Letters*, 130, pp. 504-516.

Rownaghi A.A. and Taufiq-Yap Y.H., 2010. Novel synthesis techniques for preparation of ultrahigh-crystalline vanadyl pyrophosphate as a highly selective catalyst for *n*-butane oxidation. *Industrial & Engineering Chemistry Research*, 49 (5), pp. 2135-2143.

Rownaghi A.A., Taufiq-Yap Y.H. and Rezaei F., 2010. Innovative process for the synthesis of vanadyl pyrophosphate as a highly selective catalyst for *n*-butane oxidation. *Chemical Engineering Journal*, 165, pp. 328-335.

Sant R. and Varma A., 1993. Selective oxidation of butane to maleic anhydride on a vanadium-phosphorus oxide catalyst: promotional effects of zirconium. *Journal of Catalysis*, 143, pp. 215-226.

Shen S., Zhou J., Zhang F., Zhou L. and Li R., 2002. Effect of Ce-Fe oxides additives on performance of VPO catalyst for *n*-butane oxidation to maleic anhydride in the absence of gas-phase oxygen. *Catalysis Today*, 74, pp. 37-43.

Shima K. and Hatano M., 1997. Maleic anhydride by heterogeneous oxidation of *n*-butane. *Applied Surface Science*, 121/122, pp. 454-460.

Shyamal K.B. and Rao M.S., 1992. Selective oxidation of *n*-butane to maleic anhydride; a comparative study between promoted and unpromoted VPO catalysts. *Applied Catalysis A General*, 83, pp. 149-163.

Taufiq-Yap Y.H., 2006. Effect of Cr and Co promoters addition on vanadium phosphate catalysts for mild oxidation of *n*-butane. *Journal of Natural of Gas Chemistry*, 15, pp. 144-148.

Taufiq-Yap Y.H., Leong L.K., Hussein M.Z., Irmawati R. and Abd Hamid S.B., 2004. Synthesis and characterisation of vanadyl pyrophosphate catalysts via vanadyl hydrogen phosphate sesquihydrate precursor. *Catalysis Today*, 90-95, pp. 715-722.

Taufiq-Yap Y.H., Leong L.K. and Irmawati R., 2007. *n*-Butane oxidation over γ-Al_2O_3 supported vanadium phosphate catalysts. *Journal of Natural Gas Chemistry* 16, pp. 266-272.

Trifirò, F. and Grasselli, R.K., 2014. How the yield of maleic anhydride in *n*-butane oxidation, using VPO catalysts, was improved over the years. *Topics in Catalysis*, 57 (14-16), pp.1188-1195.

Tsai W.T., 2016. Toxic volatile organic compounds (VOCs) in the atmospheric environment: regulatory aspects and monitoring in Japan and Korea. *Environments*, 3 (3), p. 23.

Wang, F., Wang, G. and Niu, X., 2016. Study on the effect of nickel doping on Mo-Bi based catalyst for selective oxidation of isobutene to methacrolein. *International Journal of Chemical Reactor Engineering*, 14(1), pp.105-112.

Waugh K.C. and Taufiq-Yap Y.H., 2003. The effect of varying the duration of the butane /air pretreatment on the morphology and reactivity of $(VO)_2P_2O_7$ catalysts. *Catalysis Today*, 81 (2), pp. 215-225.

Witko M., Tokarz R., Haber J. and Hermann K., 2001. Electronic structure of vanadyl pyrophosphate: cluster model studies. *Journal of Molecular Catalysis: A Chemical*, 166, pp. 59-72.

Xu L., Chen X., Ji W., Yan Q. and Chen Y., 2002. Influence of the way of preparing vanadium phosphorus oxide (VPO) precursor and introducing multi-additives on the reaction performance. *Reaction Kinetics and Catalysis Letters*, 76 (2), pp. 335-341.

Zazhigalov V.A., Haber J., Stoch J., Bucherikova I.V., Komashko G.A and Pyatnitskaya A.I., 1996. *n*-Butane oxidation of V-P-O catalysts: influence of alkali and alkaline-earth metal ions as additions. *Applied Catalysis A*: *General*, 134, pp. 225-237.

Website:

Felthouse, T.R., Burnett, J.C., Horrell, B., Mummey, M.J. and Kuo, Y.J., 2001. *Maleic Anhydride, Maleic Acid and Fumaric Acid* [Online].http://www.huntsman.com/petrochemicals/Media/KOMaleic.pdf. [Accessed on 20th May 2016].

APPENDICES

Appendix A

Calculation for the Gadolinium Dopant Used

Molecular weight of $VOPO_4 \cdot 2H_2O$ $= 197.9426\ gmol^{-1}$

10 g of $VOPO_4 \cdot 2H_2O$ $= \dfrac{10g}{197.9426 gmol^{-1}}$

$= 0.0505$ mol

Molecular weight of gadolinium nitrate, $Gd(NO_3)_3$,

$= 157.2500 + 3 \times [(14.0067\ gmol^{-1}) + (3 \times 15.9994\ gmol^{-1})]$

$= 343.2647\ gmol^{-1}$

Example of calculation:

For 1 mol% of Gd,

Since Gd/V = 0.01; V = 0.0505 mol

So, the concentration of Ga $= 0.000505$ mol

Total mass of Gd needed $= 0.000505\ mol \times 343.2647\ gmol^{-1}$

$= 0.173349$ g

Hence, 0.173349 g of $Gd(NO_3)_3$ was added to 10 g of $VOPO_4 \cdot 2H_2O$ to 150 cm^3 of 1-butanol and reflux at 353 K.

Calculation for the Lanthanum Dopant Used

Molecular weight of $VOPO_4 \cdot 2H_2O$ = 197.9426 $gmol^{-1}$

10 g of $VOPO_4 \cdot 2H_2O$ = $\frac{10g}{197.9426gmol^{-1}}$

= 0.0505 mol

Molecular weight of lanthanum nitrate, $La(NO_3)_3$,

= 138.9055 + 3 × [(14.0067 $gmol^{-1}$) + (3 × 15.9994 $gmol^{-1}$)]

= 324.9202 $gmol^{-1}$

Example of calculation:

For 1 mol% of La,

Since La/V = 0.01; V = 0.0505 mol

So, the concentration of La = 0.000505 mol

Total mass of La needed = 0.000505 mol × 324.9202 $gmol^{-1}$

= 0.164085 g

Hence, 0.164085 g of $La(NO_3)_3$ was added to 10 g of $VOPO_4 \cdot 2H_2O$ to 150 cm^3 of 1-butanol and reflux at 353 K.

Calculation for the Cerium Dopant Used

Molecular weight of $VOPO_4 \cdot 2H_2O$ = 197.9426 $gmol^{-1}$

10 g of $VOPO_4 \cdot 2H_2O$ = $\frac{10g}{197.9426gmol^{-1}}$

= 0.0505 mol

Molecular weight of cerium nitrate, $Ce(NO_3)_3$,

= 140.1160 + 3 × [(14.0067 $gmol^{-1}$) + (3 × 15.9994 $gmol^{-1}$)]

= 326.1307 $gmol^{-1}$

Example of calculation:

For 1 mol% of Ce,

Since Ce/V = 0.01; V = 0.0505 mol

So, the concentration of Ce = 0.000505 mol

Total mass of Ce needed = 0.000505 mol × 326.1307 $gmol^{-1}$

= 0.164696 g

Hence, 0.164696 g of $Ce(NO_3)_3$ was added to 10 g of $VOPO_4 \cdot 2H_2O$ to 150 cm^3 of 1-butanol and reflux at 353 K.

Appendix B

X-ray Diffraction (XRD) Calculations,

Crystallite size, T was calculated using to Scherrer's equation,

$$T(Å) = \frac{0.89\ \lambda}{FWHM \times \cos\theta}$$

Given $\lambda_{Cu\ K\alpha} = 1.54$ Å and FWHM (radian) = FWHM (º) $\times \frac{\pi}{180°}$,

Example of calculation steps to determine the crystallite size shown below using the Gd1Ce1 doped catalyst's data:

Plane	2θ	θ	FWHM (º)	FWHM (radian)
(0 2 0)	22.8628	11.4314	1.1191	1.9532×10^{-2}
(2 0 4)	28.4782	14.2391	0.7121	1.2428×10^{-2}

Peak appears at 2θ = 22.8628 correspond to (0 2 0) plane,

FWHM (radian) $= 1.1191º \times \frac{\pi}{180°}$

$= 1.9532 \times 10^{-2}$

$$T\ (Å) = \frac{0.89 \times 1.54\ Å}{1.9532 \times 10^{-2} \times \cos 11.4314}$$

$= 71.59$ Å

Peak appears at 2θ = 28.4782 correspond to (2 0 4) plane,

$$T\ (Å) = \frac{0.89 \times 1.54\ Å}{1.2428 \times 10^{-2} \times \cos 14.2391}$$

$= 113.78$ Å

For Gd1Ce1,

Plane	2θ	θ	FWHM (º)	FWHM (radian)
(0 2 0)	22.8628	11.4314	1.1191	1.9532×10^{-2}
(2 0 4)	28.4782	14.2391	0.7121	1.2428×10^{-2}

For Gd1Ce3,

Plane	2θ	θ	FWHM (º)	FWHM (radian)
(0 2 0)	22.8338	11.4169	1.0207	1.7815×10^{-2}
(2 0 4)	28.4803	14.2402	0.8554	1.4930×10^{-2}

For Gd1Ce5,

Plane	2θ	θ	FWHM (º)	FWHM (radian)
(0 2 0)	22.8863	11.4432	1.0017	1.7483×10^{-2}
(2 0 4)	28.7775	14.3888	1.3249	2.3124×10^{-2}

For La1Ce1,

Plane	2θ	θ	FWHM (º)	FWHM (radian)
(0 2 0)	22.8058	11.4029	1.2997	2.2684×10^{-2}
(2 0 4)	28.4247	14.2124	0.6298	1.0992×10^{-2}

For La1Ce3,

Plane	2θ	θ	FWHM (º)	FWHM (radian)
(0 2 0)	22.7981	11.3991	1.2763	2.2228×10^{-2}
(2 0 4)	28.4405	14.2203	0.6505	1.1353×10^{-2}

For La1Ce5,

Plane	2θ	θ	FWHM (º)	FWHM (radian)
(0 2 0)	22.8084	11.4042	1.1398	1.9893×10^{-2}
(2 0 4)	28.4167	14.2084	0.6798	1.1865×10^{-2}

Appendix C

BET Analysis Nitrogen Adsorption Curves

For Gd1Ce1,

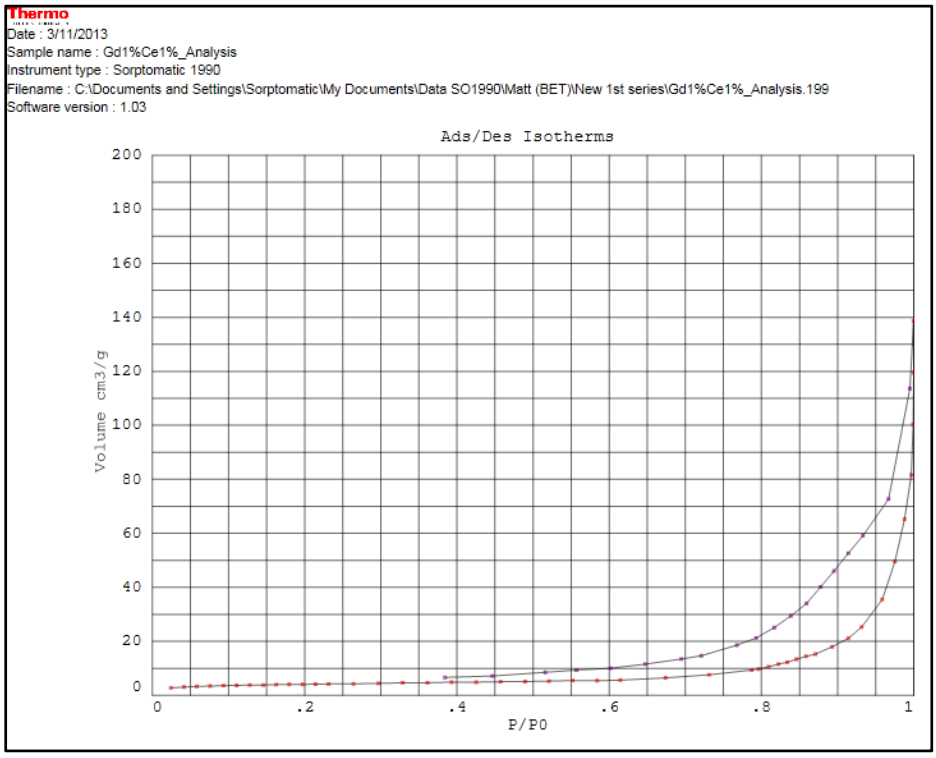

For Gd1Ce3,

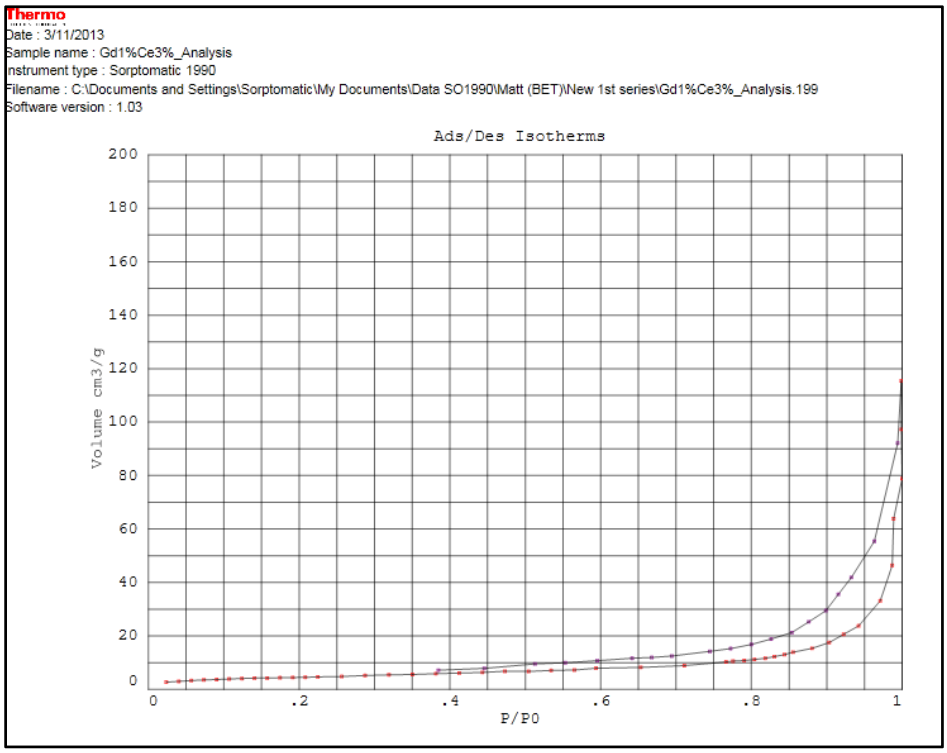

For Gd1Ce5,

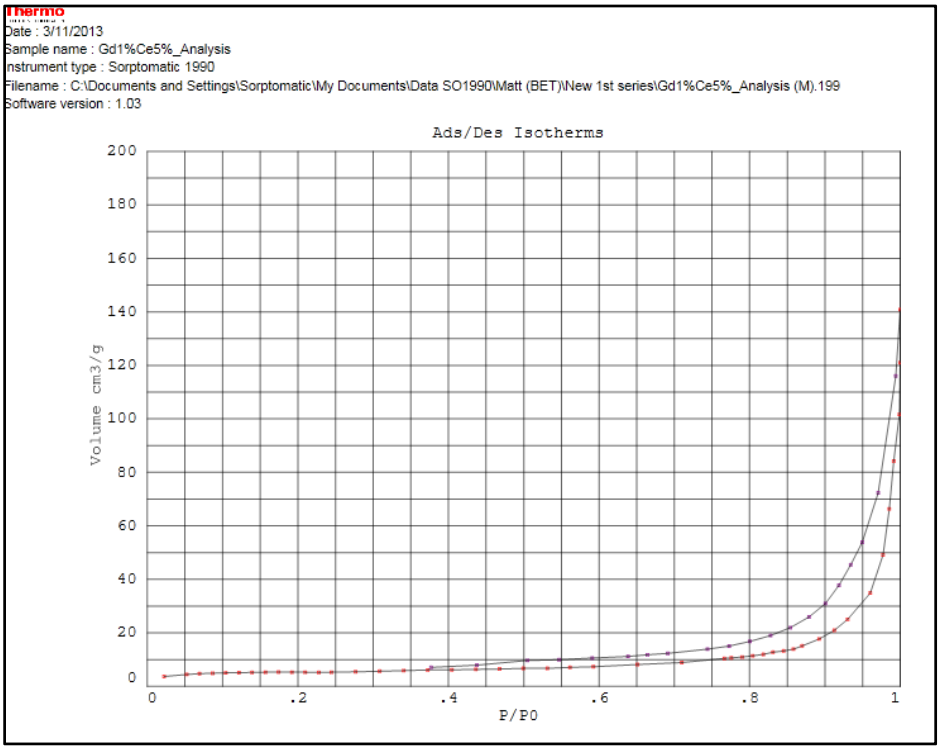

For La1Ce1,

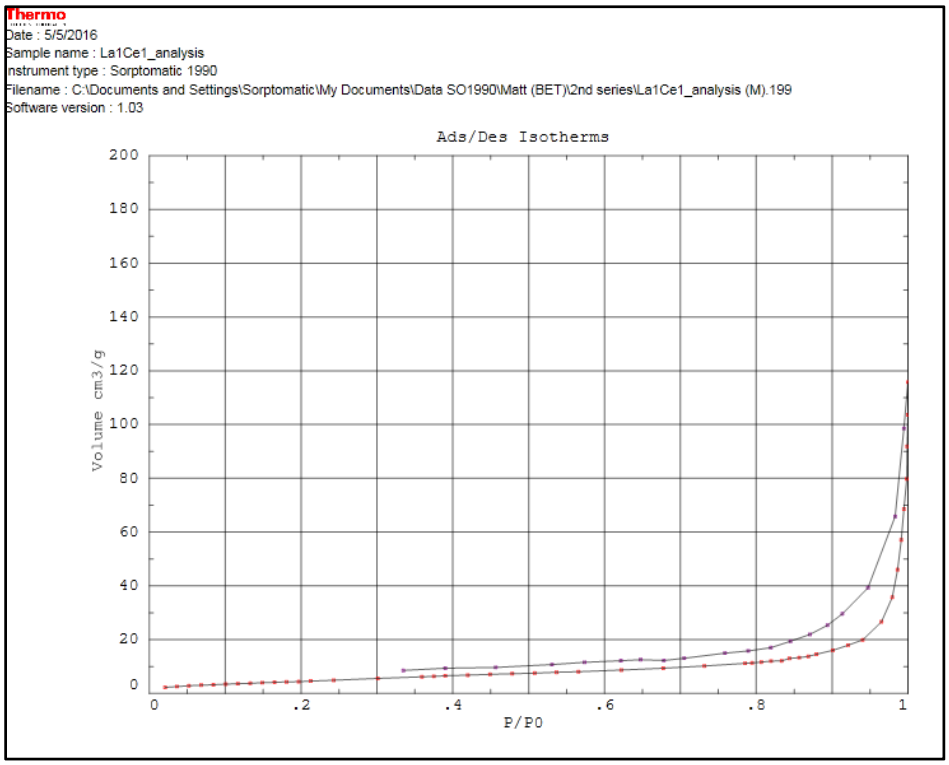

For La1Ce3,

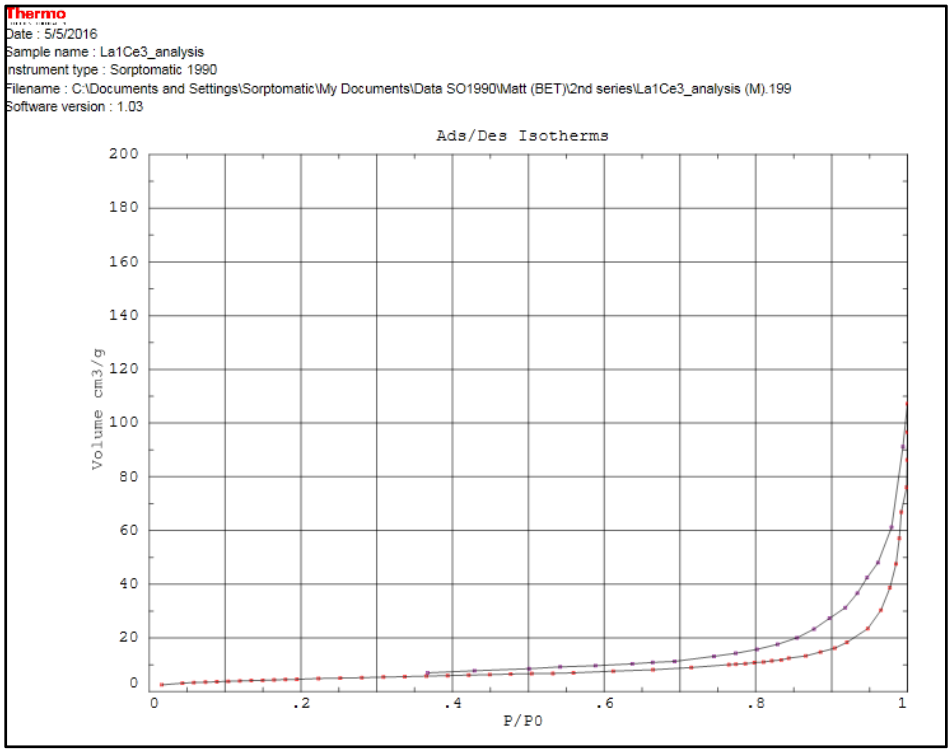

For La1Ce5,

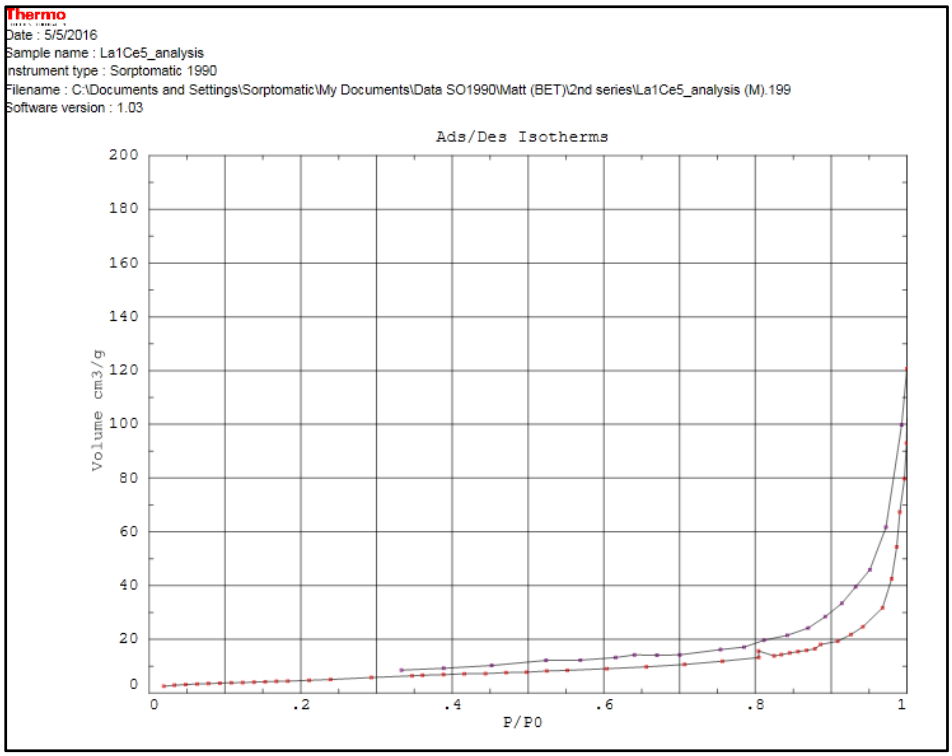
Thermo
Date : 5/5/2016
Sample name : La1Ce5_analysis
Instrument type : Sorptomatic 1990
Filename : C:\Documents and Settings\Sorptomatic\My Documents\Data SO1990\Matt (BET)\2nd series\La1Ce5_analysis (M).199
Software version : 1.03
Ads/Des Isotherms
Volume cm3/g
200
180
160
140
120
100
80
60
40
20
0
0
.2
.4
.6
.8
1
P/P0

Appendix D

Preparation of Solutions Used for ICP-OES Analysis

Preparation of 8 M HNO_3,

$$\text{Molarity for 65 \% of } HNO_3 = \frac{\text{Density of } HNO_3}{\text{Molecular Weight of } HNO_3} \times \frac{65}{100} \times 1000$$

$$= \frac{1.4090\ \text{g cm}^{-1}}{63.0130\ \text{gmol}^{-1}} \times \frac{65}{100} \times 1000$$

$$= 14.5343\ \text{mol L}^{-1}$$

$$= 14.5343\ \text{M}$$

$M_1V_1 = M_2V_2$

where,

M_1 = concentration of 65 % of HNO_3 (14.5343 M)

V_1 = volume of 65 % of HNO_3

M_2 = concentration of 8 M HNO_3

V_2 = volume of 8 M HNO_3

$$(14.5343\ \text{M})V_1 = (8\ \text{M})(250\ \text{mL})$$

$$V_1 = \frac{(8\ \text{M})(250\ \text{mL})}{14.5343\ \text{M}}$$

$$V_1 = 137.65\ \text{mL}$$

Hence, 137.65 mL of 65 % of HNO_3 was diluted to 250 mL with deionised water.

Preparation of Stock Solution of Phosphorus, P,

Molecular weight of $NH_4H_2PO_4$,

$= [14.0067 + (1.0079 \times 4) + (1.0079 \times 2) + 30.9738 + (15.9994 \times 4)]\ g\ mol^{-1}$

$= 115.0255\ g\ mol^{-1}$

Atomic weight of P = $30.9738\ g\ mol^{-1}$

50 ppm of stock solution for P = $50\ mg\ L^{-1}$

$= 0.05\ g\ L^{-1}$

$$\text{Number of mole of P} = \frac{0.05\ g\ L^{-1}}{30.9738\ g\ mol^{-1}}$$

$= 1.6145 \times 10^{-3}\ mol\ L^{-1}$

Mass of $NH_4H_2PO_4$ $= 1.6145 \times 10^{-3}\ mol\ L^{-1} \times 115.0255\ g\ mol^{-1}$

$= 0.1857\ g\ L^{-1}$

Hence, 0.1857 g of $NH_4H_2PO_4$ was transferred into 1000 mL volumetric flask and topped up with deionised water.

Preparation of Standard Solution of Phosphorus, P,

$M_1V_1 = M_2V_2$

where,

M_1 = concentration of stock solution (50 ppm)

V_1 = volume of stock solution

M_2 = concentration of standard solution

V_2 = volume of standard solution (250 mL)

Example of calculation for concentration of standard solution of 40 ppm:

$$(50 \text{ ppm})V_1 = (40 \text{ ppm})(250 \text{ mL})$$

$$V_1 = \frac{(40 \text{ ppm})(250 \text{ mL})}{50 \text{ ppm}}$$

$$V_1 = 200 \text{ mL}$$

Hence, 200 mL of stock solution of phosphorus was dissolved in 8 M HNO_3 and diluted further to 250 mL with deionised water to produce 40 ppm standard solution of phosphorus.

Preparation of Stock Solution of Vanadium, V,

Molecular weight of NH_4VO_3,

$= [14.0067 + (1.0079 \times 4) + 50.9415 + (15.9994 \times 3)]\ g\ mol^{-1}$

$= 116.9780\ g\ mol^{-1}$

Atomic weight of V = $50.9415\ g\ mol^{-1}$

50 ppm of stock solution for V = $50\ mg\ L^{-1}$

$= 0.05\ g\ L^{-1}$

$$\text{Number of mole of V} = \frac{0.05\ g\ L^{-1}}{50.9415\ g\ mol^{-1}}$$

$= 9.8152 \times 10^{-4}\ mol\ L^{-1}$

Mass of NH_4VO_3 $= 9.8152 \times 10^{-4}\ mol\ L^{-1} \times 116.9780\ g\ mol^{-1}$

$= 0.1148\ g\ L^{-1}$

Hence, 0.1148 g of NH_4VO_3 was transferred into 1000 mL volumetric flask and topped up with deionised water.

Preparation of Standard Solution of Vanadium, V,

$M_1V_1 = M_2V_2$

where,

M_1 = concentration of stock solution (50 ppm)

V_1 = volume of stock solution

M_2 = concentration of standard solution

V_2 = volume of standard solution (250 mL)

Example of calculation for concentration of standard solution of 10 ppm:

$$(50 \text{ ppm})V_1 = (10 \text{ ppm})(250 \text{ mL})$$

$$V_1 = \frac{(10 \text{ ppm})(250 \text{ mL})}{50 \text{ ppm}}$$

$$V_1 = 50 \text{ mL}$$

Hence, 50 mL of stock solution of vanadium was dissolved in 8 M HNO_3 and diluted further to 250 mL with deionised water to produce 10 ppm standard solution of vanadium.

Preparation of 100 ppm Sample Solution,

$$0.025 \text{ g sample in } 250 \text{ mL} = \frac{0.025\,\text{g}}{250\,\text{mL of } HNO_3}$$

$$= 0.1 \times 10^3 \text{ mg } L^{-1}$$

$$= 100 \text{ ppm}$$

Hence, 0.0250 g of sample was transferred into 250 mL volumetric flask and dissolved with 10 mL of 8 M HNO_3. Then, deionised water was used to top to 250 mL to produce 100 ppm sample solution.

Appendix E

Inductively Coupled Plasma-Optical Emission Spectrometry (ICP-OES)

Calculation of P/V mole ratio using ICP-OES analysis,

$$\frac{P}{V} = \frac{\text{Concentration of P/Atomic Weight of P}}{\text{Concentration of V/Atomic Weight of V}}$$

Example of calculation,

For La1Ce1,

$$\frac{P}{V} = \frac{21.3100/30.9738\ \text{mg L}^{-1}}{28.0800/50.9415\ \text{mg L}^{-1}}$$

$$= \frac{0.6880}{0.5512}$$

$$= 1.2482$$

Hence, the P/V atomic ratio for La1Ce1 is 1.25.

Appendix F

Preparation of Solutions Used in Redox Titration

Preparation of Diphenylamine, Ph_2NH indicator,

1 g of diphenylamine was weighed and dissolved in a few ml of concentrated sulphuric acid, H_2SO_4. Then, the solution was transferred to a 100 ml volumetric flask and further topped up with concentrated H_2SO_4.

Preparation of 2M sulphuric acid, H_2SO_4 solution,

Concentrated H_2SO_4 (95-98 %)

1 L = 1.84 kg = 1840 g/ 1000 cm^3

= 1.84 g/ cm^3

Molecular weight of H_2SO_4 = 2(1.00 g mol^{-1}) + 32.07 g mol^{-1} + 4(16.00 g mol^{-1})

= 98.07 g mol^{-1}

$$\text{Concentration of 95-98 \% } H_2SO_4 = \frac{1.84\ \text{g cm}^{-3}}{98.07\ \text{g mol}^{-1}} \times \frac{95}{100} \times 1000$$

= 17.82 M

$M_1V_1 = M_2V_2$

where

M_1 = concentration of 95-98 % H_2SO_4

M_2 = concentration of diluted H_2SO_4 (2 M)

V_1 = volume of 95-98 % H_2SO_4

V_2 = volume of diluted H_2SO_4 (2 M)

$(17.82\ M)(V_1) = (2\ M)(1000\ cm^3)$

$V_1 = 112.23\ cm^3$

Preparation of 0.1 M sulphuric acid, H_2SO_4 solution,

$M_1V_1 = M_2V_2$

where

M_1 = concentration of 95-98 % H_2SO_4

M_2 = concentration of diluted H_2SO_4 (2 M)

V_1 = volume of 95-98 % H_2SO_4

V_2 = volume of diluted H_2SO_4 (2 M)

$(17.82\ M)(V_1) = (0.1M)(1000\ cm^3)$

$V_1 = 5.61\ cm^3$

Preparation of 0.01 N potassium permanganate, $KMnO_4$,

Normality, N (eq L^{-1}) = M (mol L^{-1}) × n (eq mol^{-1})

$MnO^{4-} + 8\ H^{+} + 5\ e^{-} \leftrightarrow Mn^{2+} + 4\ H_2O$

$$\text{Molarity, M (mol/L)} = \frac{\text{N (eq L}^{-1})}{n\ (\text{eq mol}^{-1})}$$

$$= \frac{0.01}{5}$$

$$= 0.002 \text{ M}$$

Molecular weight for $KMnO_4$ = 39.10 g mol^{-1} + 54.94 g mol^{-1} + 4(16.00 g mol^{-1})

= 158.04 g mol^{-1}

Weight for $KMnO_4$ in 1000 cm^3 diluted (0.1 M) H_2SO_4 = 0.002 × 158.04

= 0.3161 g

Preparation of 0.01 N ammonium iron(II) sulphate, $(NH_4)_2Fe(SO_4)_2 \cdot 6H_2O$,

Normality, N (eq L^{-1}) = M (mol L^{-1}) × n (eq mol^{-1})

$Fe^{2+} + e^- \leftrightarrow Fe^{3+}$

$$\text{Molarity, M (mol/L)} = \frac{\text{N (eq L}^{-1})}{n\,(\text{eq mol}^{-1})}$$

$$= \frac{0.01}{1}$$

$$= 0.01 \text{ M}$$

Molecular weight for $(NH_4)_2Fe(SO_4)_2 \cdot 6H_2O$

= 2(14.00 g mol^{-1}) + 20(1.00 g mol^{-1}) + 55.85 g mol^{-1} + 2(32.07 g mol^{-1}) + 14(16.00 g mol^{-1})

= 391.99 g mol^{-1}

Weight for $(NH_4)_2Fe(SO_4)_2 \cdot 6H_2O$ in 1000 cm^3 diluted (0.1 M) H_2SO_4

= 0.01 × 391.99

= 3.9199 g

Appendix G

Calculation of Average Oxidation of Vanadium (V_{AV})

According to Niwa and Murakami (1982),

$T_1 = V^{4+} + 2V^{3+} = 20\ [MnO_4^-]\ V_1$ (1)

$T_2 = V^{5+} + V^{4+} + V^{3+} = 20\ [Fe^{2+}]\ V_2$ (2)

$T_3 = V^{5+} = 20\ [Fe^{2+}]\ V_3$ (3)

(2) – (3): $V^{3+} + V^{4+} = 20\ [Fe^{2+}]\ V_2 – 20[Fe^{2+}]\ V_3$ (4)

(1) – (4): $V^{3+} = 20\ [MnO_4^-]\ V_1 - 20[Fe^{2+}]\ V_2 + 20\ [Fe^{2+}]\ V_3$ (5)

Substitute (5) into (1):

$V^{4+} + 2(20\ [MnO_4^-]\ V_1 - 20\ [Fe^{2+}]\ V_2 + 20\ [Fe^{2+}]\ V_3) = 20\ [MnO_4^-]\ V_1$

$V^{4+} = 20\ [MnO_4^-]\ V_1 - 40\ [MnO_4^-]\ V_1 + 40\ [Fe^{2+}]\ V_2 - 40\ [Fe^{2+}]\ V_3$

$= 40\ [Fe^{2+}]\ V_2 - 40\ [Fe^{2+}]\ V_3 - 20\ [MnO_4^-]\ V_1$ (6)

Substitute (5) and (6) into (2):

$20\ [Fe^{2+}]\ V_2 = V^{5+} + (40\ [Fe^{2+}]\ V_2 - 40\ [Fe^{2+}]\ V_3 - 20\ [MnO_4^-]\ V_1) + (20\ [MnO_4^-]$

$V_1 - 20\ [Fe^{2+}]\ V_2 + 20\ [Fe^{2+}]\ V_3)$

$V^{5+} = 20\ [Fe^{2+}]\ V_3$ (7)

From (5): $V^{3+} = 20\ (0.01)\ V_1 - 20\ (0.01)\ V_2 + 20\ (0.01)\ V_3$

$= 0.2\ V_1 - 0.2\ V_2 + 0.2\ V_3$ (8)

From (6): $V^{4+} = 40\ (0.01)\ V_2 - 40\ (0.01)\ V_3 - 20\ (0.01)\ V_1$

$= 0.4\ V_2 - 0.4\ V_3 - 0.2\ V_1$ (9)

From (7): $V^{5+} = 20\ (0.01)\ V_3$

$= 0.2\ V_3$ (10)

The average vanadium valence, V_{AV} calculated as:

$$V_{AV} = \frac{3V^{3+} + 4V^{4+} + 5V^{5+}}{V^{3+} + V^{4+} + V^{5+}} \quad (11)$$

Calculation steps to determine the average oxidation state of vanadium are shown as below for Gd1Ce1,

$V_1 = 9.9$

$V_2 = 11.5$

$V_3 = 0.9$

From (5): $V^{3+} = 20\ (0.01)\ V_1 - 20\ (0.01)\ V_2 + 20\ (0.01)\ V_3$

$= 0.2\ V_1 - 0.2\ V_2 + 0.2\ V_3$

$= 0.2\ (9.9) - 0.2\ (11.5) + 0.2\ (0.9)$

$= -0.14$ (ignored)

From (6): V^{4+} $= 40\ (0.01)\ V_2 - 40\ (0.01)\ V_3 - 20\ (0.01)\ V_1$

$= 0.4\ V_2 - 0.4\ V_3 - 0.2\ V_1$

$= 0.4\ (11.5) - 0.4\ (0.9) - 0.2\ (9.9)$

$= 2.26$

From (7): V^{5+} $= 20\ (0.01)\ V_3$

$= 0.2\ V_3$

$= 0.2\ (0.9)$

$= 0.18$

The average vanadium valence for Gd1Ce1 is calculated as:

$$V_{AV} = \frac{3V^{3+} + 4V^{4+} + 5V^{5+}}{V^{3+} + V^{4+} + V^{5+}}$$

Since the value of V^{3+} is negative, it was ignored.

$$V_{AV} = \frac{3(0) + 4(2.26) + 5(0.18)}{0 + 2.26 + 0.18}$$

$= 4.0738$

Since V_{AV} of Gd1Ce1 is 4.0738,

Hence, V^{5+} $= 7.38\ \%$

V^{4+} $= (100 - 7.38)\ \%$

$= 92.62\ \%$

Appendix H

Calculation of TPR in H_2 Analysis

Total oxygen removed (atom g^{-1})

= Amount of oxygen removed (μ mol g^{-1}) $\times$ 6.022×10^{23} atom mol^{-1}

= Amount of oxygen removed (atom g^{-1})

Example of calculation:

For Gd1Ce1,

Total oxygen atom removed = (1135.4520 + 2312.9891) μ mol g^{-1}

= 3.4484×10^{-3} mol g^{-1}

= 3.4484×10^{-3} mol $g^{-1} \times 6.022 \times 10^{23}$ atom mol^{-1}

= 2.0766×10^{21} atom g^{-1}

Appendix I

Calculation of Reduction Activation Energy (E_r) for TPR in H_2 Analysis

Calculation step to obtain reduction activation energy, E_r,

$$H_2\,(c) + O\,(s) \rightarrow H_2O\,(g) + \lambda$$

where

(s) = surface or lattice oxygen species

(c) = chemisorbed species

(g) = gaseous species

λ = oxygen vacancy

$$\text{Rate} = k[H_2]m[O_s]$$

$$-\frac{d[H_2]}{dt} = A\exp\left(\frac{d[H_2]}{dt}\right)[H_2]_m[O_s] \qquad (1)$$

Setting the derivative of equation (1) to zero at T_m gives the modified version of Redhead (1962) equation:

$$\frac{E_r}{RT_m^{\,2}} = \left(\frac{A_r}{\beta}\right)[H_2]_m \exp\left(\frac{-E_r}{RT_m}\right) \qquad (2)$$

From the Arrhenius (1889) equation,

$$k_1 = A\exp\left(\frac{-E_r}{RT_m}\right) \tag{3}$$

Thus, from equation (2),

$$k_2 = A[H_2]_m \exp\left(\frac{-E_r}{RT_m}\right) \tag{4}$$

Since k_1 and k_2 are the same at T_m and let k = χ at T_m,

$$\frac{\chi}{A[H_2]_m} = \exp\left(\frac{-E_r}{RT_m}\right) \text{ or } \left(\frac{A[H_2]_m}{\chi}\right) = \exp\left(\frac{E_r}{RT_m}\right)$$

$$\frac{E_r}{RT_m} = \ln\left(\frac{A[H_2]_m}{\chi}\right)$$

$$E_r = RT_m \ln\left(\frac{A[H_2]_m}{\chi}\right)$$

where

R = 0.001987 kcal K^{-1} mol^{-1}; 82.056 cm^3 atm K^{-1} mol^{-1}

A = 10^{13} s^{-1}

T_m = maximum temperature of the peak

E_r = reduction activation energy